UNIVERSITY OF OKLAHOMA

GRADUATE COLLEGE

HOT SURFACE IGNITION PROPERTIES OF PRE-VAPORIZED JET-A AND ITS BLENDS WITH SOY METHYL ESTER AND CANOLA METHYL ESTER IN A CONSTANT VOLUME CHAMBER

A THESIS

SUBMITTED TO THE GRADUATE FACULTY

in partial fulfillment of the requirements for the

Degree of

MASTER OF SCIENCE

By

BACH DUONG
Norman, Oklahoma
2019

HOT SURFACE IGNITION PROPERTIES OF PRE-VAPORIZED JET-A AND ITS BLENDS WITH SOY METHYL ESTER AND CANOLA METHYL ESTER IN A CONSTANT VOLUME CHAMBER

A THESIS APPROVED FOR THE
SCHOOL OF AEROSPACE AND MECHANICAL ENGINEERING

BY

Dr. Ramkumar Parthasarathy, Chair

Dr. Wilson Merchan-Merchan

Dr. Hamidreza Shabgard

This thesis is dedicated to my family and friends for their unconditional love and support

"Stay hungry. Stay foolish."
Steve Jobs

ACKNOWLEDGEMENTS

I would like to express my deepest gratitude and appreciation to my committee chair, Dr. Ramkumar Parthasarathy, who has been an incredible mentor and my greatest support. I have always been greatly amazed by his carefulness, highly organized style, and excitement in regard to teaching. Working with him has been a privilege and it has helped me grow a lot personally and professionally. Without his guidance and continual support in the last two years, this thesis would not have been possible.

I would like to thank Dr. Gollahalli for his life time dedication to the Combustion and Flame Dynamics Laboratory, where my research was conducted.

I would like to thank Dr. Wilson Merchan-Merchan and Dr. Hamidzera Shabgard for being part of my thesis defense committee. I truly enjoyed the courses and the talks I had with you two.

I would like to thank Scott Carter, for his initial construction of the setup; Alex Spens for his instructions and for helping me become familiar with the setup; Shaik Zehad and Tanner Mann for their assistance collecting and analyzing data. Also huge thanks to Billy Mays and Greg Williams from AME machine shop for their aid in maintaining the setup.

I would like to thank Arun Balakrishnan, Flavio Moreno, and Tonci Maleta for their welcome and support when I first came to the lab.

A special thanks to Nhi Nguyen, for her care and support.

Finally, I would like to thank my parents, Nhan and Dong, for their love and encouragement; my little brother, Tung, for his humor and late night talks even though he is living halfway across the world.

TABLE OF CONTENTS

LIST OF TABLES

LIST OF FIGURES

ABSTRACT

In recent years, biofuels have emerged as an attractive alternative to traditional petroleum fuels due to their renewable and almost carbon-neutral nature. While the fundamental ignition properties of petroleum fuels are well understood, knowledge of ignition properties of biofuels and their blends with petroleum fuels is limited. Studies of the fundamental ignition properties of biofuels are important for the safety of storage and transportation of these fuels. The objective of this study was to compare the relative hot surface ignition properties of biofuel blends at different equivalence ratios in a constant-volume chamber. Properties that were measured in this study are: ignition energy, time interval for ignition, ignition surface temperature, and flame front velocities. The fuels studied were blends of Jet A (petroleum fuel), Soy Methyl Ester, and Canola Methyl Ester (biofuel) over an equivalence ratio range of 0.75-2.0. A commercially available silicon carbide dryer ignitor was used as the ignition source and was located in the center of the combustion chamber. A high-speed camera recorded the propagation of the flame following ignition, allowing for the calculation of the flame front velocity. K-type thermocouples measured the temperature of the mixture at selected points inside the combustion chamber.

The flames produced by the blends propagated quickly and were brightest at equivalence ratios of 1.3 – 1.5. For all the blends, the power supplied to the ignitor increased gradually and became stagnant as it approached the ignition point. It was also found that the time interval for ignition decreased with increasing equivalence ratio. Ignition temperature of the air-fuel mixture was nearly constant for all fuels at about 650^{O}C (923 K). Upper and lower flame velocity peaked at around 6.5 m/s and 3.2 m/s,

respectively, at equivalence ratios of 1.3 – 1.5. In general, ignition properties of biofuel blends were comparable to those of their pure fuels.

CHAPTER 1: INTRODUCTION

The Monthly Energy Review report produced by the Unites States Energy Information Administration (2019) showed that in the first 11 months of 2018, fossil fuels accounted for approximately 80% of energy consumed in the United States, whereas renewable energy including hydroelectric, geothermal, solar, wind, and biomass power finished second with 11.5%, and the remaining came from nuclear power. The fossil fuels including coal, natural gas, and crude oil are burned to produce electricity, or are refined to produce new products for heating and transportation. The report also stated that in the same period the use of fossil fuels produced more than 4.8 billion metric tons of carbon dioxide (CO_2) as an exhaust, and this built up to approximately 81% of greenhouse gas emissions in the United States, consequently contributing to the climate change. In particular, fossil fuels used in transportation sector, which consumed 28% of the total energy, produced up to 1.7 billion metric tons of CO_2 (United States Energy Information Administration, 2017). It is fundamentally important, therefore, to seek alternative sources of fuel that are more environmentally-friendly than petroleum fuels.

While it takes a lot of time to shift to new energy sources, adopting clean fuels with similar properties to traditional fossil fuels is a viable solution. Biodiesel has emerged to be one of those fuels and has become increasingly popular in the last few decades (National Biodiesel Board, 2019). Biodiesel is a biofuel that is produced from the transesterification of vegetable or other oils. Transesterification is a process through which vegetable oils are turned into methyl esters with the help of a catalyst such as potassium hydroxide. Biodiesels, such as Soy Methyl Ester (SME), Canola Methyl Ester (CME), and Palm Methyl Ester (PME), have gradually become more popular as a clean

energy source. The blends of these biofuels and petroleum fuels such as diesel and Jet A fuel are currently used as transportation fuels. The advantages of these fuels over petroleum fuels are that they are produced from renewable sources and are nearly carbon-neutral. Carbon-neutral is the term to describe the process at which the CO_2 absorbed by the feedstocks of biodiesel such as rapeseed, soybeans, and palm trees offsets the CO_2 produced during the making and consuming of biodiesel. However, biodiesel is not always generating positive environmental impacts. Land that is reserved for food and forest planting has been cleared to grow those feedstocks to create biodiesel in some developing countries (The Guardian, 2014). This could potentially outweigh the benefits of using SME, CME, or PME fuels.

Due to the similarity of their properties to those of petroleum fuels, biodiesel can be readily blended with petroleum fuels and used in existing diesel engines with no or minimal modifications. Several studies have been conducted to document the performance of these biofuels and biofuel blends on engine performance. These studies have been primarily concerned with the emissions from engines with the use of biofuels and their blends. One of the fundamental characteristics of combustion is ignition. Leaking of flammable fluids onto hot surface of machinery components could cause fires and even explosions. A report by U.S. Air Force stated that there are over 100 engine fires every year (Bennett et al., 2003). This number is also comparable in commercial aircrafts. Majority of these fires are ignited by ruptured fuel, oil or hydraulic pipes, causing the fluids to contact hot engine components. Fire prevention systems must take into account the problems of hot surface ignition. An in-depth study into this area will help increase the understanding of the combustion of biofuel blends in addition to

assisting in devising safety procedures while handling biofuels and biofuel blends in aircraft and automobile tanks, pipelines and other structures.

The objective of this work is to compare ignition properties of biofuel blends of SME and CME at various of equivalence ratios. Previous research on biofuel blend flames has shown that variables such as NOx emission index display a non-monotonic behavior with volume concentration of biofuel in the blends (Balakrishnan et al, 2016). Therefore, the goal was to document the hot surface ignition temperature, ignition energy, time interval of ignition and flame velocities of vaporized Jet A/SME and Jet A/CME blends at three volume ratios of 25%-75%, 50%-50%, 75%-25%, and compare them with the values obtained by Spens (2017) for pure Jet A, pure SME and CME. The fuel blends used in the experiment was in an equivalence ratio range of 0.75 to 2.00. As mentioned above, the results from this study would become extremely useful in designing mechanical components and updating safety parameters for handling and storing these blends.

CHAPTER 2: LITERATURE REVIEW

Ignition methods such as auto-ignition and spark-ignition of various air-fuel mixtures have been studied in detail by several authors such as Lewis and von Elbe (1961), Myronuk (1980), and Sheperd et al. (1999). In the same time, hot-surface ignition studies have been limited. Zabetakis et al. (1954) investigated the minimum ignition temperature of various hydrocarbons using the hot surface ignition method. The chamber was a 200 cc Erlenmeyer flask heated by a 1200W electric crucible heater. The hydrocarbon fuels including methane, JP-4, and paraffin hydrocarbons were injected into the flask through a syringe and the ignition was observed visually. The results showed a trend between ignition temperature and the chain length of the paraffin hydrocarbons. It was observed that as the chain length increased, the minimum temperature for ignition decreased. Specifically, methane with one Carbon atom experienced an ignition temperature of $537^{O}C$, while n-hexadecane with the average chain length of 16 only observed $205^{O}C$ ignition temperature. The time delay before ignition was found to decrease as the ignition temperature increased. The time delay decreased from 140 s to 5 s when the ignition temperature increased from $200^{O}C$ to $400^{O}C$ for paraffin hydrocarbons.

To improve safety of working conditions in coal mines, the British Ministry of Power Safety in Mines Establishment funded Rae et al. in 1964 to conduct experiments on the ignition of methane-air mixtures due to heated surfaces. The research focused on the effect of ignition with varying surface area and orientation of the ignition source, which was an electrically heated aluminum square. The sizes varied from 3x3 mm^2 to 18x18 mm^2 while the locations were at the floor, roof or the wall of the combustion

chamber. The ignition temperatures were obtained by lowering the surface temperature until ignition occurred and were measured using an optical pyrometer. The results showed that the minimum ignition temperature decreased with increasing surface area. In particular, for the surface area of 9 (3x3) mm^2, the minimum ignition temperatures were 1361^OC, 1390^OC, 1400^OC at the floor, roof, and wall of the chamber, respectively. With the size increased to 81 (9x9) mm^2, ignition temperatures were 1156^OC, 1200^OC, and 1219^OC and with maximum surface area of 324 (18x18) mm^2, they were 1070^OC, 1090^OC, and 1141^OC. The authors did not provide any explanation to the significance of this result.

Kutcha et al. (1965) compared the hot surface ignition temperature of heat sources of different sizes for hydrocarbon fuel vapors and air. The combustion chambers included cylinders and spheres with varying radii between 0.4 and 1.75 cm, and 1.0 to 3.7 cm, respectively. The experiments were performed under atmospheric pressure. Tested fuels included n-hexane, n-octane, n-decane, JP-6, and aircraft engine oil. The results showed that the auto-ignition temperature (AIT) decreased with increasing fuel molecular weight, and with decreasing surface to volume ratio. Particularly, it was found that the auto-ignition temperature (AIT) in a 10 cm^3 sphere of n-hexane with a molecular weight of 86 g/mol and n-decane with a molecular weight of 142 g/mol was at approximately 509^OC and 427^OC, respectively. The AIT of JP-6 decreased from 596^OC to 242^OC as its surface area to volume ratio dropped from 5.15 cm^{-1} to 1.25 cm^{-1}. The authors explained that the heat release during combustion depended on the wall surface area. As the surface area to volume decreased, the energy release from the walls would drop, resulting in smaller thermal energy to reach the AIT.

Kuchta and Cato (1966) investigated the hot gas ignition of hydrocarbon fuel vapor-air mixtures in a pipe chamber of 4-inch diameter and 26 inch long. The heat source was a Platinum-Rhodium wire wrapped in a ceramic tube. Chromel-alumel thermocouples were used to measure the temperature of the vapor-air mixtures. The fuel used was JP-6, which was then injected into the chamber through a mixing ring. Jet diameter and fuel-to-air mass ratio was varied in the experiment. It was found that the ignition temperature decreased with increasing jet diameter. For JP-6, 1/8-inch jet diameter required an ignition temperature of 1085^{O}C, while ¾ inch jet diameter only required 699^{O}C. Varying the fuel-to-air mass ratio from 0.3 to 0.7, had little impact on the ignition temperature of JP-6. For the cases of fuel-to-air ratio less than 0.3, the ignition temperatures were found to increase by 5%. The authors suggested that the unusually high fuel-to-air ratios were ignitable due to the dilution caused by the hot air jet. Compared to other ignition methods, the temperature of hot gas ignition was 93^{O}C and 149^{O}C higher than that of heated wire and heated vessel.

Cutler (1974) examined the ignition probability of methane and propane air mixtures using a tungsten strip as the ignition source. The studied parameters included the size, temperature and the heating rate of the strip, which had a fixed length of 31.7 mm, thickness of 0.03 mm, and varying width from 4.8 to 11.9 mm. The peak temperature was obtained in 0.5 milliseconds and was measured by an optical pyrometer. It was found that as the strip width increased, the ignition temperature decreased and the 7% of methane/air mixture had the highest probability of ignition, while the lowest probability was measured on the 3.3% propane/air mixture. Specifically, the ignition temperature of 7% methane/air dropped from 1850 to 1680^{O}C as the strip width increased

from 4.8 to 11.9 mm. In a similar manner, the ignition temperature of 3.3% propane/air decreased from 1373^{O}C to 1273^{O}C when the strip width increased from 6.4 to 11 mm. Cutler then drew a conclusion that the ignition probability would be greater if the ignition source was kept longer in a flammable mixture at a given temperature.

Onu et al. in 1976 analyzed the ignition temperature in a free convection flow of an electrically vertical heated surface, consisting of a 18-8 chromium-nickel steel plate. The plate had the dimensions of 0.3 mm think, 40 mm wide and varying length between 5 and 30 mm. A stoichiometric mixture of methane and propane was injected into a pressurized chamber ranging from 0.07 to 1 atm. After heating up the ignition source to just under the ignition temperature, the surface was then heated slowly until the flame propagation was observed. The ignition temperature was defined as the temperature immediately before the ignition. Ignition delay was not taken into consideration. It was reported that the ignition temperature decreased with the concentration of the propane/air mixture, and the minimum ignitable concentration was 2.25%. When the initial mixture temperature decreased, the ignition temperature increased. Specifically, at 60^{O}C of initial temperature, the ignition temperature was measured at 927^{O}C-1127^{O}C.

Botteri et al. (1979) examined ignition of vaporized Jet A, using results reported by Macdonald and Cansdale (1972) and Kuchta, et al. (1965). The experiments were conducted under atmospheric pressure in a 46 cm radius heated sphere. The ignition sources were pipes with various sizes. For the same outer sphere temperature of 25^{O}C, the ignition temperature was found to be 350^{O}C and 700^{O}C for the pipe diameter of 152 mm and 19 mm, respectively. When the outer sphere temperature increased to 200^{O}C, ignition temperature also increased from 275^{O}C to 350^{O}C as the pipe diameter decreased

from 152 mm to 19 mm. The conclusion of this research was that the smaller surface area of ignitor led to a greater required ignition temperature. This result could be explained by a smaller temperature gradient of the mixture close to the ignitor for a smaller surface area. This small temperature gradient lowered the thermal energy provided to the mixture.

Johnson et al. (1988) performed testing in the Aircraft Engine Nacelle Fire Test Simulator (AENFTS) in order to measure the minimum hot surface ignition temperature (MHSIT) of several aircraft fuels including JP-4 and JP-8. The fuels were sprayed onto different locations on the hot bleed-air duct of a F-16 right side engine compartment simulation, which was installed in the AENFTS. The F-16 nacelle simulator adopted an early prototype of the F-100 engine, which was then modified to fit in the AENFTS. Nitrogen gas was used to pressurize the fluid reservoirs of the fuel delivery system. The reservoirs were pressurized from 105 to 135 psi for 8 ml/s spray flowrate. Air pressure, temperature, velocity, and fuel flowrate were the varying parameters that affected the MHSIT. It was found that when JP-4 was sprayed at 8 ml/s with 1 and 2 ft/s of airflow rate, the MHSIT reached a temperature of approximately 621^{O}C, whereas MHSIT of JP-8 was found to be around 593^{O}C when the fuel being sprayed at 8 ml/s with airflow rate of 2 ft/s.

Siccana et al. (1993) investigated the ignition of ethane-oxygen-nitrogen, with varying parameters including gas velocity and the temperature of the electrically heated wire made from kanthal-A1 (which is an alloy of mainly Fe, Cr and Al) of 0.6mm in diameter and 40mm long. The wire was placed vertically in the chamber. The experiment was conducted on the fuel-rich side, at room temperature and pressure of 10 atm. The

mixture was injected upwardly into the chamber at a speed of around 80 cm/sec, through a stainless-steel test tube of an inner diameter of 2 1mm and a length of 2.5m. If the chamber pressure increased more than 0.25 atm, the ignition was considered to have occurred. In reality, the pressure rise was up to 3 atm during the ignition. It was also reported that the ignition occurred within the first 20 seconds after heating up the kanthal-A1 wire. During the experiments, based on temperature, three different regimes were observed, i.e. negligible reaction, local reaction and ignition. Temperature around 700^{O}C characterized the regime of negligible reaction. At a high temperatures 900^{O}C -1,000^{O}C, the mixture near the wire started to react. Ignition occurred almost immediately at temperatures higher than 1,000^{O}C. At the transition of negligible reaction to local reaction a jump of 200^{O}C in the temperature was observed. The authors explained that the transition between local reaction to ignition depended on the balance between the heat production and heat removal, and ignition occurred when the heat generated by the chemical reaction near the wire was larger than the heat removed. The heat loss was mainly due to convection. It was also observed that the faster the mixture passed the hot wire, the higher the temperature required to cause ignition as a certain amount of the gas must reach a certain temperature in order to form radicals and initiate a chemical reaction. Another important observation was that at the moment the gas flow was stopped ignition occurred. This observation was made during the first tests when a stoichiometric mixture of ethane-air flowed upward through a stainless-steel tube with an inner diameter of 50mm, pressure *5* atm and a mixture velocity of 10 cm/sec. The size and temperature of the ignition source used in these tests were 0.1mm in diameter and 20mm long and 1,200^{O}C respectively.

Duarte (1994) investigated the effect of "local confinement" on the ignition of flammable mixture at a hot surface. Electrically heated nichrome strips served as heating surfaces and were placed in a vessel to measure the minimum temperature required to cause ignition of a 3 % propane/air mixture. The results showed that the ignition temperature decreased as the depth of the confinement was increased. Specifically, at 10 mm, 20mm, and 40 mm deep, the ignition temperature was found at $870^{O}C$-$890^{O}C$, $850^{O}C$-$870^{O}C$, and $800^{O}C$-$820^{O}C$, respectively. This result was verified using the Frank-Kameneskii thermal theory for a static flammable mixture within a closed vessel. The effect of lowering the ignition temperature relating to the depth of the cavity could be influenced by the following factors: due to the upwards orientation of the hot surface, the sides of the cavity would impede the buoyancy induced flow and increase the convective time of the mixture; the ceramic fibreboard used in the setup served as an excellent insulation, thus significantly reducing the heat loss.

Kong et al. (1995) et al examined the AIT of several types of hydrocarbon mixtures including CH_4 air, C_3H_8 air, CH_4/C_3H_8/air, and CH_4/air/CO_2. Temperature of the homogeneous gas mixtures was measured using an 11-ignition bomb. The bomb was placed inside an oven of 10kW power to adjust the temperature. Using results of previous tests, the oven temperature was set a value slightly below the anticipated AIT. As the bomb wall reached the desired temperature, the gas mixture was injected in the form of a turbulent jet. Ignition was observed when the pressure inside the bomb saw a sudden rise. It was found that the minimum AIT of CH_4 air was found at around $640^{O}C$ in the equivalence ratio range of 0.30-0.83, whereas that of C_3H_8 air was at $500^{O}C$ corresponding to equivalence ratio of 2.79-4.04. For CH_4/C_3H_8/air, the AIT decreased

monotonically with increasing C_3H_8 concentration in the fuel mixture. Specifically, for equivalence ratio of 0.75, AIT dropped from 640^OC to 540^OC as the concentration increased from 0 to 100%, while AIT of equivalence ratio of 2.34 decreased from 540^OC to 505^OC as the concentration increased from 20 to 100%.

Kermit et al. (1997) studied the ignition temperature of hydrocarbon fuels under atmospheric pressure conditions. The controlled parameters included the fuel/air stoichiometry, properties of heated metal surface, and the contact time between the mixture and the surface. The experiments were conducted on 15 hydrocarbon fuels containing 1 to 8 carbon atoms on heated nickel, stainless steel, and titanium surfaces for three difference equivalence ratios (0.7, 1.0 and 1.3). The results showed that autoignition temperatures were about 500 K higher than prior investigations, where exposure time was longer. The autoignition temperature decreased for larger hydrocarbons and for richer mixtures. For example, on nickel surface, methane at equivalence ratio of 0.7 had an ignition temperature of 1367^OC and 1247^OC at equivalence ratio of 1.3. Similarly, butane had autoignition temperatures at 1201^OC and 1228^OC at equivalence ratios of 0.7 and 1.3 respectively. It was also found that branched alkanes were more difficult to be ignited than their linear isomers. In terms of surface properties, nickel was associated with the highest autoignition temperature while stainless steel was observed to have the lowest.

Ma et al. (1998) investigated the combustion characteristics of methane-air mixtures initiated by laser sparks. The combustion chamber was a high-pressure Otto-cycle single-cylinder of diameter of 88.9 mm. The piston stroke with a length of 96.5 mm and a compression ratio of 12.2 was driven by an electric motor hydraulic ram. The laser beam was operated at three different wavelengths was produced from krypton fluoride

gas (= 248 nm), argon fluoride gas (= 193 nm), and a Nd:YAG laser beam (= 1064 nm). The beam focused into the combustion chamber by a planoconvex synthetic fused silica lens to ignite the methane-air mixtures. By the end of the experiment, the results showed that laser-induced ignition produced a 4-6 ms decrease in time for combustion to reach peak pressure compared to ignition initiated by electric spark and glowplug spark in the same chamber and under the same conditions, which was verified using Raizer's theory in calculating the kernel size and breakdown velocity.

Shaw et al. (2009) studied the ignition temperature of gasoline, diesel, and bio-diesel fuels on hot surfaces. To measure surface temperatures, and to record the evaporation and ignition events, infrared thermography method was adopted. The bio-diesel fuels used in this study included soy-based diesel and tallow-containing diesel. The fuels were sprayed as single droplets into two different surfaces: 409 stainless steel and a stainless steel heat shield. The experimental results showed that the MHSIT of gasoline on stainless steel was 520^{O}C, and 660^{O}C for 100% ignition probability. Both traditional diesel and bio-diesel experienced similar MHSIT at around 450^{O}C, and 500^{O}C for 100% ignition probability. However, 100% soy-based bio-diesel demonstrated a more hostile ignition behavior on the heated shield surface. This indicated that the hot surface properties such as material type, shape, and age became significant in determining the MHSIT and ignition probabilities of different fuels.

McGray et al. (2011) investigated the ignition temperature and the rate of energy generation of CME and SME bio-diesel fuels in oxygen-nitrogen mixtures in a heated plug flow reactor. A 90% platinum (Pt) 10% rhodium (Rh) wire with 127 mm of diameter was coiled and placed in the quartz tube of the reactor to serve as the catalyst. The

absolute volume fraction of fuel ranged from 0.238% to 0.445% while the equivalence ratio varied between 0.4 and 1.0. The fuel was evaporated by heated nitrogen and then mixed with oxygen. The mixture was injected into the reactor where the Pt-Rh wire was electrically heated. It was found that the ignition temperatures increased with increasing equivalence ratio and volume fraction of fuel vapor. At equivalence ratio of 0.4 and 0.268% volume fraction, the ignition temperature of SME was recorded at $639^{O}C$, whereas that of CME was found at $718^{O}C$ at equivalence ratio of 1.0 and 0.445% volume fraction. The rate of energy release for both bio-diesels was found to decrease with increasing equivalence ratio and decreasing fuel volume fraction. For CME, the energy release reached its lowest of 6.9 W/cm^2 at equivalence ratio of 1 for 0.268% fuel and its highest of 25.3 W/cm^2 at equivalence ratio of 0.4 for 0.445% fuel. For the case of SME, lowest and highest energy release was 5.1 W/cm^2 and 28.6 W/cm^2 at equivalence ratio of 0.4 with 0.268% and 0.417% fuel, respectively.

Boettcher (2012) investigated the constant-volume hot surface ignition of n-hexane air mixtures in detail with a glowplug mounted inside a combustion chamber of 11.4 cm x 11.4cm x 17.1 cm. A highspeed camera was used to record the flame propagation. The heat source is a Bosch glowplug of 3.1mm diameter and an Autolite 1110 glowplug of 5.1 mm diameter. Temperatures of the top of the case and of the glowplug were measured using K-type thermocouples with 0.5 second response time. The equivalence ratio of the mixtures was varied from 0.25 to 2.75. Away from the lower flammability temperature, the ignition temperature was nearly constant at around $661^{O}C$ (934 K) for a range of equivalence ratios 0.75-2.6. It was reported that the flame velocities reached a maximum of 5.5 m/s for the top velocity and 3.0 m/s for the side

velocities around equivalence ratios of 1.2. The theory proposed that the upper flame velocity was higher than the sides due to the strong convective flow generated due to buoyancy above the glowplug.

Stanthopoulos et al. (2013) examined the hot wire ignition of ethanol-oxygen hydrothermal flames. To generate the ignition, a water-ethanol mixture was used as fuel while gaseous oxygen was treated as oxidizer. The combustion chamber was pressured at 260 bar. A Ni/Cr 60/15 coiled wire of 2.5 mm diameter, 0.4 mm thickness and 30mm length was used as the ignition source due to its high temperature robustness and chemical compatibility. The results showed that higher ethanol concentration mixtures produced lower ignition powers. In particular, 12.5% ethanol mixture required 220W of power where 17.5% mixture only required 150W. The ignition temperature also behaved in a similar manner. Ignition temperatures were found at 775^{O}C and 730^{O}C for 12.5% and 17.5% ethanol mixture, respectively. The dependence on ethanol concentration of ignition temperature was much weaker than on ignition power, which was supported by prior studies.

Spens (2017) studied the hot-surface ignition of Jet A and canola methyl ester (CME) in a constant volume chamber. The rectangular combustion chamber (7 cm by 7 cm by 33cm high) had a viewing window in the front. Liquid fuel was injected into a stream of hot air, vaporized and mixed, and the fuel/air mixture was passed through the combustion chamber vertically upward. The combustion chamber was filled with mixtures of various equivalence ratios. A 120V dryer heating element was mounted horizontally at the center of the chamber and served as the hot surface. The power input to the hot surface, the temperatures at different locations inside the chamber and images

obtained from a high-speed camera were recorded simultaneously. The ignition delay, ignition energy and flame velocities were documented over a range of equivalence ratios with Jet A and CME as fuels. The ignition delay and ignition energy reached minimum values around equivalence ratios of 1.1-1.3. Spens (2017) documented the hot surface ignition temperature, ignition delay and ignition energy of soy methyl ester (SME) and palm methyl ester (PME) in the same set-up. The hot surface ignition temperature was found to be nearly constant at 630 ^{O}C (903 K) for all the fuels over the range of equivalence ratios of 0.75-2.0. The ignition time interval and the ignition energy of the biofuels were comparable to those of Jet A. The flame velocities recorded on the top half of the chamber were significantly higher than those recorded in the bottom half due to buoyancy effects.

The objective of this study is to extend the investigation of Spens (2017) to biofuel blends with Jet A. In the past, it has been shown that combustion properties of blends are non-monotonic functions of the volume concentrations of the fuels. Therefore, the ignition energy, ignition delay and the flame velocities were recorded for SME-Jet A blends and CME-Jet A blends.

CHAPTER 3: EXPERIMENTAL SETUP

3.1. Experimental Setup

Experiments were conducted at the Combustion and Flame Dynamics Laboratory of the University of Oklahoma. In order for the flue gases not to leak into the laboratory setup and devices, the pressure inside the laboratory was intentionally set lower than the atmospheric pressure to create a positive draft.

The setup consisted of a metal combustion chamber, an air/fuel delivery system, several heating tapes, a highspeed camera to capture flame images, and a National Instruments data acquisition system (NI-DAQ) to collect and analyze data parameters such as ignition temperature, ignition energy. It was also equipped with a 20-cm diameter fume hood for exhaust purpose.

A constant volume chamber setup was constructed to study the ignition properties of pre-vaporized liquid fuels. Air and fuel of predetermined rates were mixed and heat up using electrical heating tapes prior to combustion and were delivered into the chamber through an air/fuel delivery system. The NI-DAQ and a laptop computer with LabVIEW software installed and with the highspeed camera connected were used for data acquisition, controlling the mixture and chamber temperature. Figure 3.1 shows overall setup, including combustion chamber surrounded by steel walls, the laptop connected to DAQ device, exhaust to the fume hood, high speed camera, and fuel pump system using a syringe. It also shows the view from the high-speed camera to the chamber through the glass window. Figure 3.2 shows a schematic diagram of the combustion chamber and inflow tubing.

3.1.1. Combustion Chamber

The combustion chamber had internal dimensions of 7.0 cm x 7.0 cm x 32.0 cm and a volume of approximately 1.56 litters. Figure 3.3 displays a schematic diagram of the combustion chamber. Chamber walls were made of steel with one face made of high temperature rated glass in order for the combustion process to be recorded by high speed camera. A thin steel sheath was wrapped around the chamber with space in between. This volume was then filled with insulation material which was the cotton fiber. There was a 1.3 cm diameter opening at the bottom of the chamber as the injection of air-fuel mixture. Above this inlet was a diffuser plate that helped distribute the mixture evenly into the chamber. Ignitor and thermocouples were mounted at the back of the chamber through a hollow cylinder of 6.0 cm inner diameter, 0.1 cm thickness and 3.0 cm depth. The exhaust from the chamber went through a steel hollow cylinder at the back, 5 cm above the ignitor mounting position, which connected to the fume hood to deliver the exhaust out of the laboratory.

3.1.2. Ignitor

The ignitor used in the combustion chamber was the same type from commercial dryers, this is due to being easily acquired and uniformly manufactured. The ignitor was controlled by a relay which connected it to a standard 115-120 V power outlet. The heating element was constructed out of silicon carbide, with a specific heat of 670 J/ kg K and a density of 3.21 g/cm^3 (Gieck & Gieck, 1990). The volume of the exposed heating element was 1.45 cm^3 with a surface area of 17.8 cm^2. A schematic diagram of the ignitor can be found in Figure 3.4. The location of the ignitor is the combustion chamber is displayed in Figure 3.2 and Figure 3.3.

3.1.3. Air/Fuel Delivery System

Air used in the combustion process was provided by the laboratory compressor and went through pressure gauge to ensure that it remains at a constant pressure of 10 psi. Following the pressure gauge, the air flowed through a LO FLO 1/4-33-G-5 rotameter with a stainless steel ball float. The rotameter had a range of up to 38 L/min and was incremented in marks of 1% of maximum flow rate. Corrections were made to account for the higher pressure of the air resulting in a corrected maximum flow rate of 31.21 L/min (McCrometer, 1996). The air passed through a process heater locating 1 meter below the chamber, and then was heated up to approximately 375°C. This temperature was found to be sufficient to vaporize the fuel for complete combustion and leaving no coking in the tubes (Balakrishnan et al., 2016).

At 7 cm below the process heater, liquid fuel was mixed into the air through a Harvard Apparatus band electronic pump system using a syringe and an injection needle. Fuel flow rate was input from the control panel of the system. A wet piece of cloth was wrapped around the fuel tube and needle interface to prevent the plastic tube from melting due to high temperature at the process heater, where the needle was connected to. Air-fuel mixture flowed vertically upwards through a steel tube of 1.3 cm diameter wrapped by heating tape. This was to keep the tube at 375°C, to vaporize the fuel. Both the process heater and heating tape were controlled by the DAQ and LabVIEW program through relays that connected to a 220 V AC wall power supply. A diagram of the air/fuel delivery system is presented in Figure 3.5.

3.2. Data Collection and Analysis

Data collection was conducted using the DAQ device and LabVIEW software, whereas images of the combustion captured by high speed camera was collected though MotionPro software. Figure 3.6 provides an overview of the control system and data collection system used in the setup. Each of the seven graphs in LabVIEW correlates to a variable which was measured. These included voltage readings in the ignitor, temperature of fuel injection, temperature at various points in the combustion chamber. Below the thermocouple temperature graphs, on the right side, is the camera trigger voltage, which was measured in Volts and used to determine when the highspeed camera was triggered. MotionPro was set at specific frame rate, exposure time, and recording style of the camera to produce the highest quality of captured images.

3.2.1. Power and Energy Measurements

The power used by the ignitor was measured using a current transformer and shunt resistor. A current transformer with 442 coils was attached to one of the power lines of the ignitor, which was then connected to a 240 ohm shunt resistor. The voltage was measured on each side of the resistor by the DAQ. The power of the ignitor was determined by multiplying the current and the voltage, which was assumed to be 120 Volt. LabVIEW performed these calculations at a rate of 100 samples per second.

Integrating the power obtained above over time would gave the ignition energy of the ignitor, given in the following equation:

$$E_{ignition} = \int_{t_0}^{t_{ignition}} P_{ignitor}\, dt \qquad 3.1$$

Where t is the time in seconds and P is the power of the ignitor in Watts. The method used was the trapezoidal Riemann sums and the raw data was recorded by the DAQ and

LabVIEW. It was tested by a voltmeter that for the first 3 seconds, the voltage across the ignitor was not 120 V (as assumed), but a constant value of 115 V AC. Hence, the following correction was made to obtain the proper value of energy through ignitor:

$$E_{115V} = E_{120V} \times \frac{115}{120} \quad 3.2$$

Where E_{115V} is the energy calculated, in Joules, correctly using a wall voltage of 115 V and E_{120V} is the energy calculated, in Joules, incorrectly using a wall voltage of 120 V.

Not all of the energy consumed by the ignitor was transferred to the fuel-air mixture; a correction must be made due to the energy lost due to radiation.

The energy lost to radiation can be determined using the Stefan-Boltzmann law, for radiation power, integrated with respect to time (Wong, 2003). The emissivity of the material of the ignitor was assumed to be 1.0.

$$E_{R\ (radiation)} = \int_{t}^{t_i} A\sigma[(T_i(t))^4 - (T_{case}(t))^4]\, dt \quad 3.3$$

Where σ is the Stefan-Boltzmann constant 5.67 x 10-8 $W/m^2\ K^{-4}$, A is the surface area of the ignitor, T_i is the temperature of the ignitor as a function of time in Kelvin, and T_{case} is the temperature of the case as a function of time in Kelvin, and t_i the time of ignition in seconds. The case temperature can be treated as a constant and is set by the initial case thermocouple temperature.

After obtaining the energy loss due to radiation and energy required to heat up the ignitor, the adjusted ignition energy was calculated as following:

$$E_{adjusted} = E_{ignition\ (115V)} - E_R \quad 3.4$$

Where $E_{ignition\ (115V)}$ is the previously calculated ignition energy in Joules, adjusted for the correct wall voltage, E_R is the energy lost by radiation in Joules.

3.2.2. Mixture Temperature Measurements

The temperature of the mixture was measured using Omega brand K-type, chromel-alumel junction, thermocouples, with grounded stainless steel sheaths of diameter 1.5 mm. Thermocouples were placed at three different locations in the setup: upstream measurement was taken prior to the entrance of the combustion chamber, other two measurements were taken at the center of the combustion chamber near the ignitor with one placing at 1 mm above the ignitor and the other placing at 15 mm above the ignitor. If at any time during the experiment the upstream measurement read a temperature below 375°C, the LabVIEW would initiate the heating tape and the process heater via a relay to quickly rise the temperature of the mixture back to 375°C. These thermocouples measured the temperature at a rate of 1000 Hz. An overview of their locations relative to the ignitor is displayed in Figure 3.2, cross section A-A.

3.2.3. Surface Temperature Measurements

The interior wall temperature was measured using an omega brand K-type thermocouple, inserted through the back plate near where the ignitor was mounted, and bent to touch the back wall at a point 5.5 cm below the ignitor. Similar to the mixture temperature measurements, when this thermocouple sensed a temperature below 350°C, the LabVIEW would activate the cartridge heaters through a relay to heat up the chamber.

The surface temperature of the ignitor was calculated indirectly using the resistance of the ignitor that varied with temperature (Spens, 2017). The resistance of the ignitor at the measured temperature was determined by the initial current that passed through the ignitor. This was repeated 68 times over a variety of temperatures ranging

from 22°C to 1100°C. The temperature was then plotted in Excel, as a function of current. Applying a best fit polynomial produced the following equations:

$$T_i(I) = 5.4I^5 - 94.3I^4 + 642.0I^3 - 2122.4I^2 + 3548.2I - 2234.5 \quad 3.5$$

$$T_i(I) = -447.8I^2 + 4184.1I - 8684.3 \quad 3.6$$

Where T_i is the temperature of the ignitor, in °C, and I is the instantaneous current flowing through the ignitor, in amps. Due to the nature of the current-temperature relations of the ignitor, Equation 3.5 was used in the case of steady current or increasing current with time, whereas Equation 3.6 applied in the case of decreasing current with time. It was approximated that at around 700°C, the current through ignitor began decreasing with time. When the ignitor was turned on, it was found that its temperature increased linearly with time. This observation was used with Equation 3.3 to determine the radiation energy released by the ignitor.

3.2.4. Flame Front Velocity Measurements

The velocity of the flames was determined from the images recorded by a highspeed camera. This camera is an IDT brand MotionPro X3 with a maximum rate of 1000 frames per second. LabVIEW software was programmed to trigger the camera through a 5V voltage output from the DAQ. To sync the camera frames with temperature and power data, the trigger cable was also connected back to the DAQ. The highspeed camera frame rate was set at 500 Hz and an exposure of 1997 microseconds for the majority of the trials.

After each trial, a series of images were saved that captured a few second period before and after the ignition. These images were then analyzed to calculate the flame front velocities including upper and lower velocities. For the distance reference, a set of

1.0 cm sized markings was placed on the left side of the combustion chamber window. The upper and lower flame front velocities were calculated by using the change in distance and the change in time between the first appearance of a flame, and the furthest measurable distance by the equation:

$$V_{flame\ front} = \frac{(h_{last\ flame\ temperature} - h_{first\ flame\ temperature}) \times fps}{(n_{last\ flame\ temperature} - n_{first\ flame\ temperature})} \quad 3.7$$

Where $V_{flame\ front}$ is the velocity of the flame front in m/s, h is the height of the flame, as measured as the absolute value of the distance from the ignitor to the flame front in meters, n is the frame number, and fps is the frame rate in frames per second.

It was observed that there was a large difference between the measured upper and lower flame velocities. This could be explained by the significant buoyant forces acting on the gases inside the combustion chamber after combustion. The following equation calculates the velocity of the airflow at a certain location within the combustion chamber due to buoyancy effect:

$$V_{gas} = \frac{(h_{last\ ember\ temperature} - h_{first\ ember\ temperature}) \times fps}{(n_{last\ ember\ temperature} - n_{first\ ember\ temperature})} \quad 3.8$$

Where V_{gas} is the local velocity of the gas in m/s, h is the ember's height from the bottom of the viewing window, n is the frame number as captured by the highspeed camera, and fps is the frame rate in frames per second.

3.2.5. Other Measurements

The time interval for ignition was an important parament that required the knowledge of the moment ignition took place. It was defined that the first visual appearance of a flame captured by the highspeed camera marked the occurrence of ignition. The time of ignition in the collected data could calculated by the equation:

$$t_{ignition} = t_{recording\ started} + \frac{n_{ignition}}{fps} \quad 3.9$$

Where $t_{ignition}$ is the time of ignition in seconds relative to the start of the DAQ data recording, $t_{recording}$ started is the time of triggering of the highspeed camera in seconds relative to the start of the data recording, $n_{ignition}$ is the frame number of the first observed flame, and fps is the frame rate in frames per second.

The time interval for ignition was calculated using the difference between the time the ignitor was activated and ignition using the equation:

$$\Delta t_{for\ ignition} = t_{ignition} + t_{0\ (ignitor\ enabled)} \quad 3.10$$

Where $\Delta t_{for\ ignition}$ is the time interval for ignition in seconds, $t_{ignition}$ is the time in seconds at which ignition occurred, and $t_{0\ (ignitor\ enabled)}$ is the time in seconds at which the ignitor was activated. The time interval for ignition was calculated during data analysis.

3.2.6. Uncertainties

For each blend, the experiments were repeated at least four times for one equivalence ratio. Uncertainties were calculated from the results using standard methods based on the Student-t distribution with a 95% confidence value. A table of typical uncertainties can be found in Table 3.3. Uncertainties are also marked as error bars in figures containing results.

3.3. Test Procedures

3.3.1. Heat-Up Phase

Before each run, the setup went through a heat-up process, in which the air in the air-fuel delivery system was heated to a temperature of 375°C (648 K) by heating tape. The combustion chamber temperature was also increased to 350°C (623 K) through the

process heater to prevent the condensation of the fuel on the walls during the fueling phase. During the heat-up process, the bypass valve was closed, the exhaust was connected to the vent hood in non-operating state. The heat-up phase took approximately 30 minutes for the first trial and 5 minutes for every trial after that.

3.3.2. Filling Phase

Once the setup was heated to desired temperatures, the filling phase initiated. Using a syringe bump, fuel was injected into the air-fuel pipe to form a pre-vaporized mixture for a duration of 1 minute. The pump and the airflow were then switched off simultaneously. The highspeed camera recording was also started in the MotionPro software on computer.

3.3.3. Ignition Phase

The ignition phase began after the filling process. During this transition, several actions were required to be performed simultaneously to best trap the fuel air mixture in the chamber: placing the exhaust hose in the bypass pipe while opening the valve to let the air flow from the chamber to the pipe, capping the exhaust with an aluminum foil cap, turning off the fuel pump and airflow system to isolate the chamber, and removing the glass insulation for photo capture. Next, the heating tape and process heaters were turned off; a current passage was sent to the ignitor until the ignition occurred. The camera was then triggered to take images. Lastly, the ignitor was turned off, ending the data recording. Temperature measurements and all the flame images were recorded. The whole process lasted about 2 minutes before returning to heat-up phase for another trial.

3.4. Test conditions

Table 3.2 shows the list of properties of tested fuel, including density, air to fuel stoichiometric ratio, heating values. For simplicity in naming the blends, J, S, C stand for Jet mA, SME, and CME. For instance, 75J25S stands for the blend of 75% of Jet A and 25% of SME in terms of volume concentration. The biofuels tested have oxygen content on average of 11% by mass, significantly greater than Jet A, which has none. The adiabatic flame temperature is comparable between Jet A and biofuels but unknown for their blends; the lower heating value of the blends lie in between Jet A and biofuels. Since SME contains more double bonds than CME, combustion characteristics between the two fuels are different, such as higher NOx emission in laminar prevaporized SME flames than the corresponding CME flames (Love et al., 2009). This indicates that even though the physical properties of biofuel blends can be determined, their ignition and combustion properties remain unknown and need to be studied.

In this experiment, the airflow rate was kept constant and the fuel flow rate was increased to increase the equivalence ratio. The fuel flow rate for each fuel at each equivalence ratio is presented in Table 3.4.

Table 3.1: List of equipment

Equipment	**Manufacturer**	**Version / Specifications**
Laptop Computer	Sony	Vavio
Data Acquisition Unit	National Instruments	SCB-68
Rotameter	S.K. McCrometer	LO FLO ¼-33-G-5 with a Stainless-Steel Float
Pressure Gauge	U.S. Gauge	-
Ignitor	Whirlpool	279311
Syringe Pump	Harvard Apparatus	55-2222

Table 3.2: Properties of tested fuels (Balakrishnan, 2017)

Fuel	**Molecular Formula**	**Molecular Weight (kg/kmole)**	**Density (kg/m^3) at 24 °C**	**Adiabatic Flame Temperature at Stoichiometric Conditions (K)**	**Air/Fuel Stoichiometric Ratio**	**Lower Heating Value (MJ/kg)**	**Boiling Point (°C)**
Jet A	$C_{13}H_{23}$	179	796	2207	14.380	42.8	145-310
Soy Methyl Ester (SME)	$C_{18.8}H_{34.6}O_2$	292.2	881	2216	12.427	37.0	351-405
75J25S	$C_{14.1}H_{25.2}O_{0.4}$	201	813	-	13.851	41.3	-
50J50S	$C_{15.4}H_{27.7}O_{0.8}$	225.8	834	-	13.350	39.9	-
25J75S	$C_{16.9}H_{30.8}O_{1.3}$	255.3	855	-	12.876	38.4	-
Canola Methyl Ester (CME)	$C_{19}H_{36}O_2$	296	876	2216	12.522	37.4	340-405
75J25C	$C_{14.1}H_{25.4}O_{0.4}$	201	815	-	13.879	41.4	-
50J50C	$C_{15.4}H_{28.2}O_{0.8}$	225.8	836	-	13.403	40.0	-
25J75C	$C_{16.9}H_{31.7}O_{1.3}$	255.3	861	-	12.952	38.7	-

Table 3.3: Typical estimated experimental uncertainties

Measurement	Typical Uncertainty
Measured Ignition Energy	±119.19 J
Time Interval for Ignition	±0.24 s
Upper Flame Front Velocity	±0.87 m/s
Lower Flame Front Velocity	±0.80 m/s
Adjusted Ignition Energy	±116 J
Ignition Temperature	±34.7°C

Table 3.4: Fuel flow rates for varying equivalence ratios

Equivalence Ratio	Airflow Rate (L/min)	Jet A (mL/min)	75J25S (mL/min)	50J50S (mL/min)	25J75S (mL/min)	SME (mL/min)
0.75	30.3	2.39	2.43	2.46	2.48	2.48
1.00	30.3	3.19	2.59	2.62	2.65	3.31
1.10	30.3	3.51	2.91	2.95	2.98	3.64
1.20	30.3	3.83	3.24	3.27	3.31	3.97
1.30	30.3	4.14	3.56	3.60	3.64	4.30
1.40	30.3	4.46	3.88	3.93	3.97	4.63
1.50	30.3	4.78	4.05	4.09	4.14	4.97
1.75	30.3	5.58	4.21	4.26	4.30	5.79
2.00	30.3	6.38	4.53	4.58	4.64	6.62

Equivalence Ratio	Airflow Rate (L/min)	Jet A (mL/min)	75J25C (mL/min)	50J50C (mL/min)	25J75C (mL/min)	CME (mL/min)
0.75	30.3	2.39	2.42	2.50	2.59	2.49
1.00	30.3	3.19	3.22	3.34	3.45	3.33
1.10	30.3	3.51	3.54	3.67	3.80	3.66
1.20	30.3	3.83	3.87	4.00	4.14	3.99
1.30	30.3	4.14	4.19	4.34	4.49	4.32
1.40	30.3	4.46	4.51	4.67	4.83	4.66
1.50	30.3	4.78	4.83	5.00	5.18	4.99
1.75	30.3	5.58	5.64	5.84	6.04	5.82
2.00	30.3	6.38	6.44	6.67	6.91	6.65

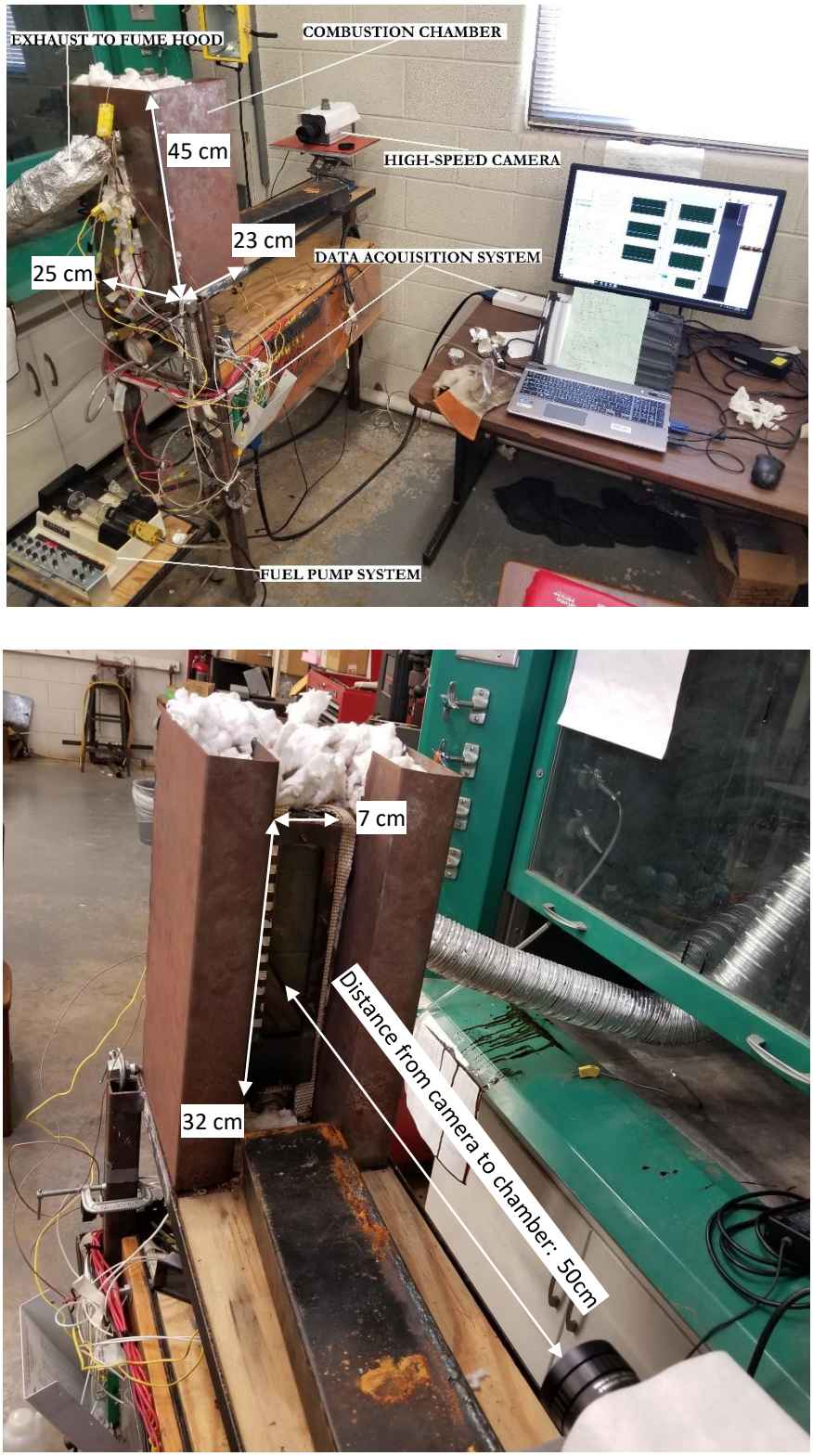

Figure 3.1: Images of the setup

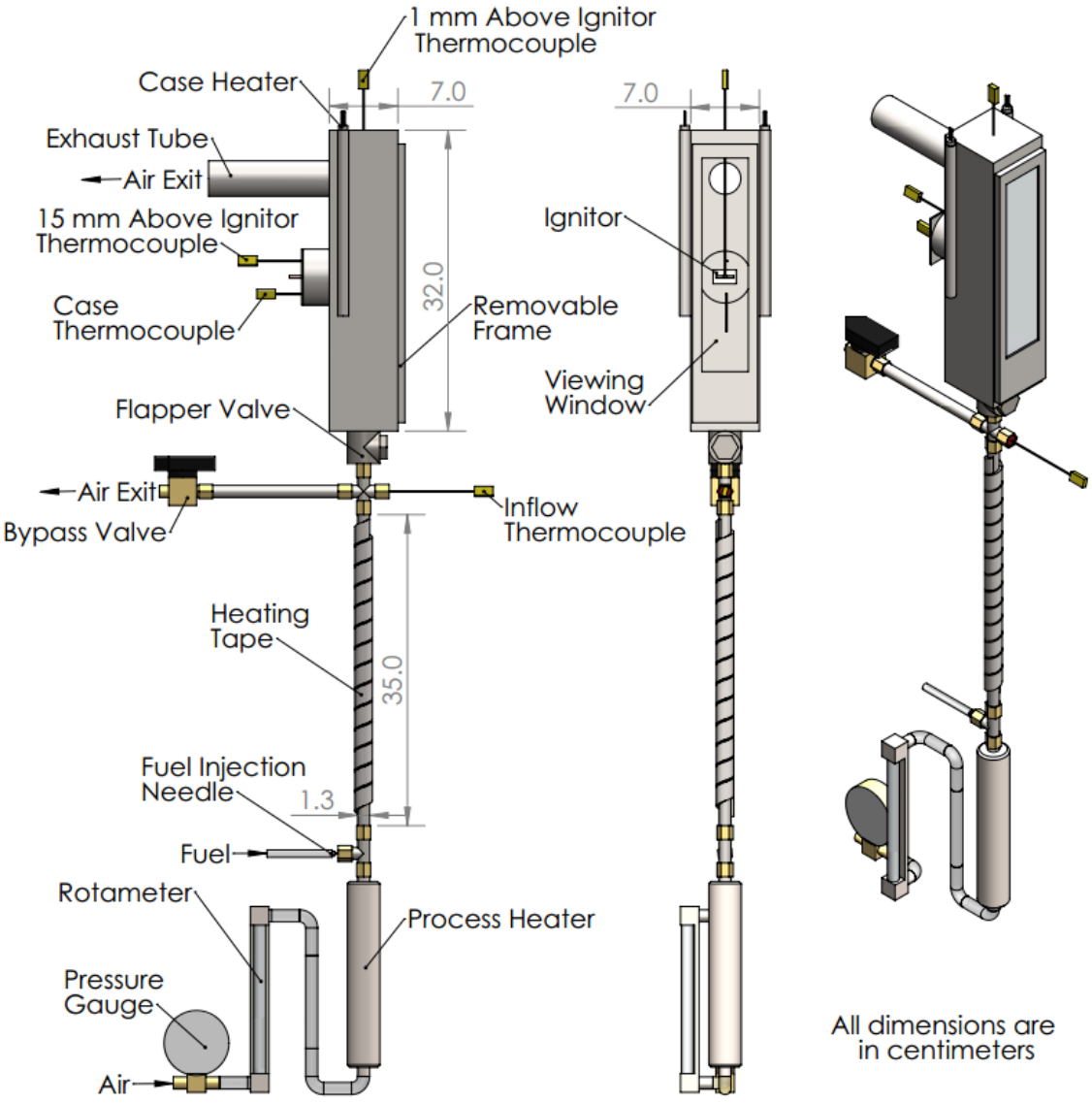

Figure 3.2: Combustion chamber and tubing diagram

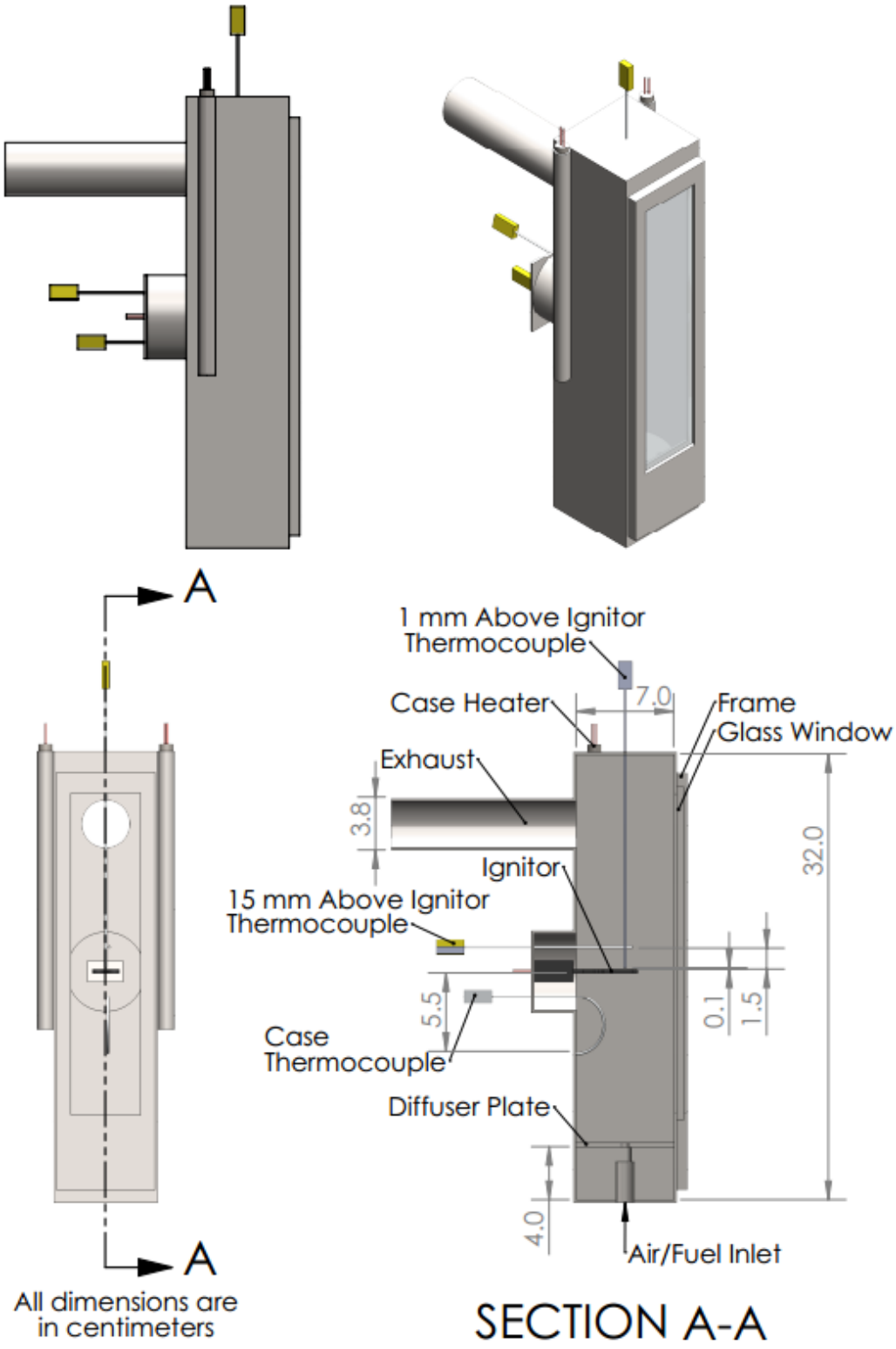

Figure 3.3: Combustion chamber diagram

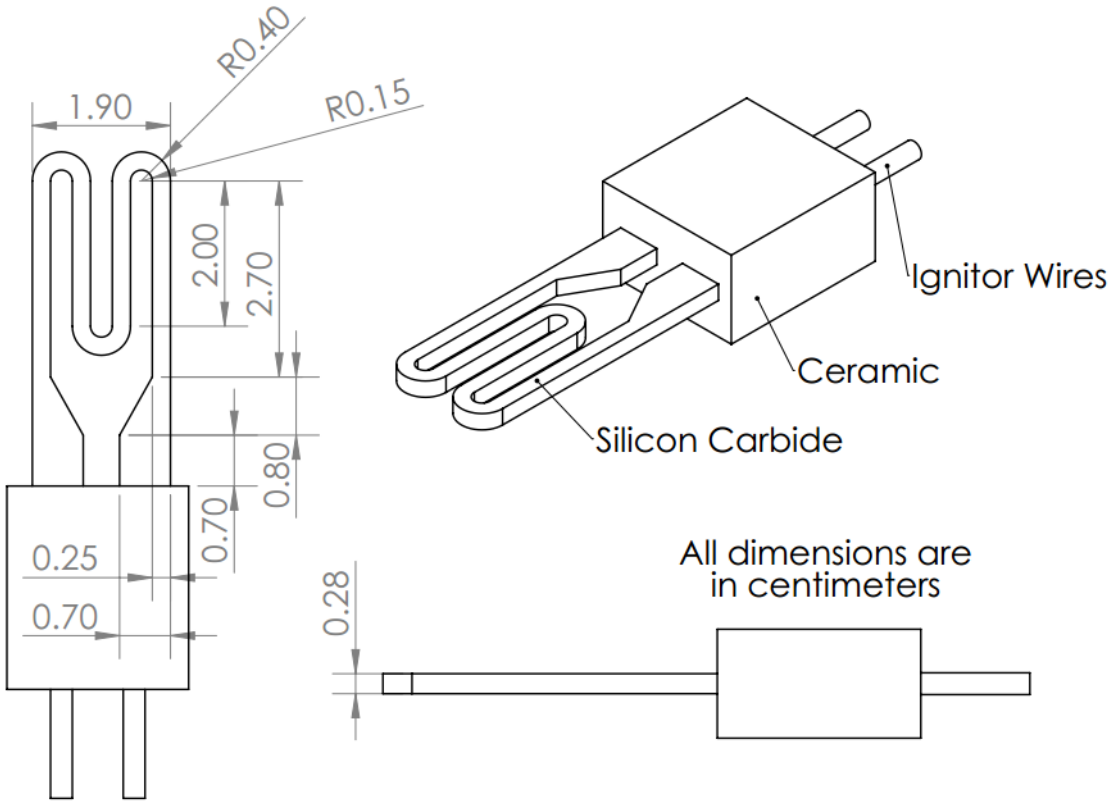

Figure 3.4: Ignitor Schematic

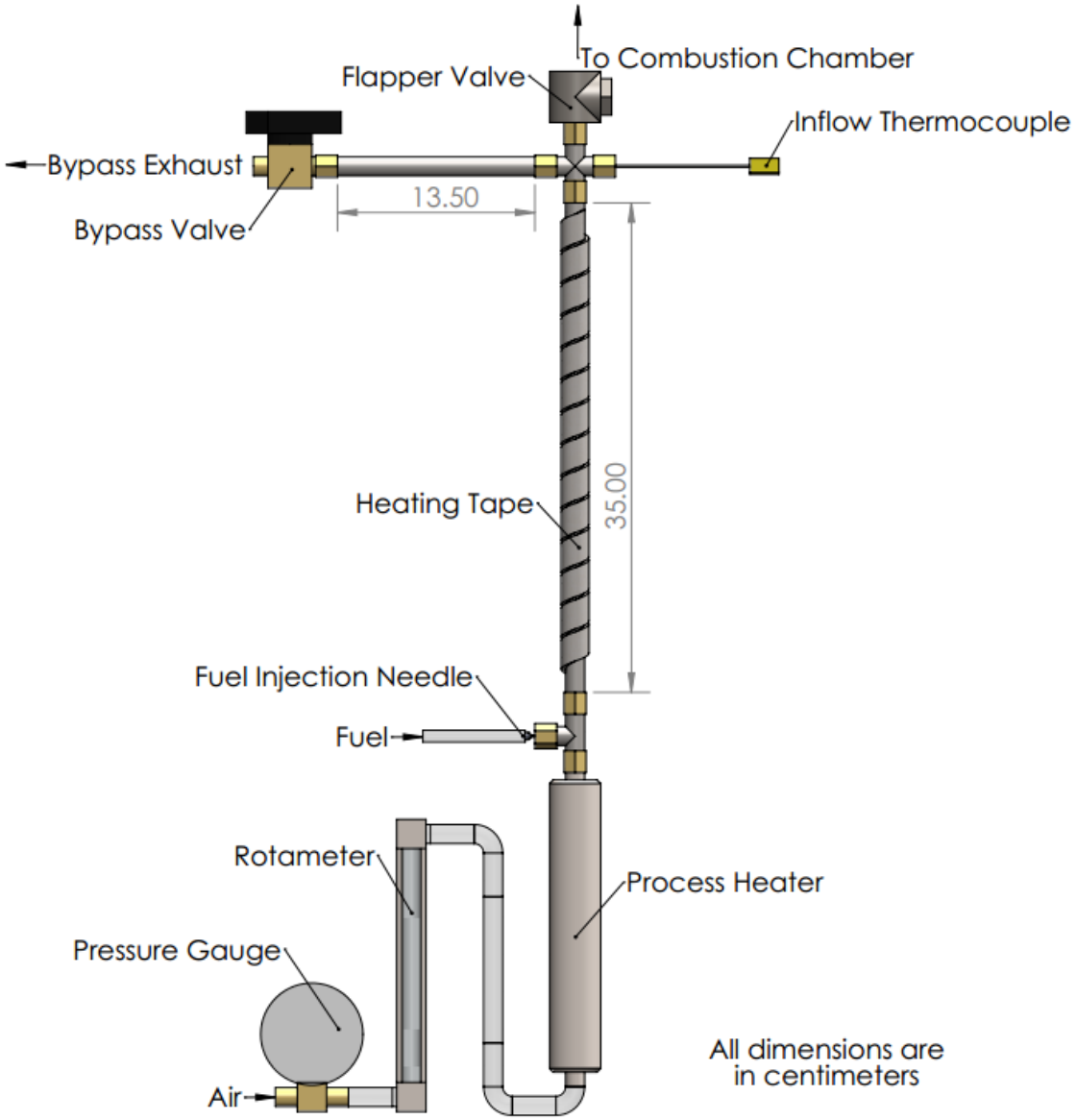

Figure 3.5: Air/fuel delivery system diagram

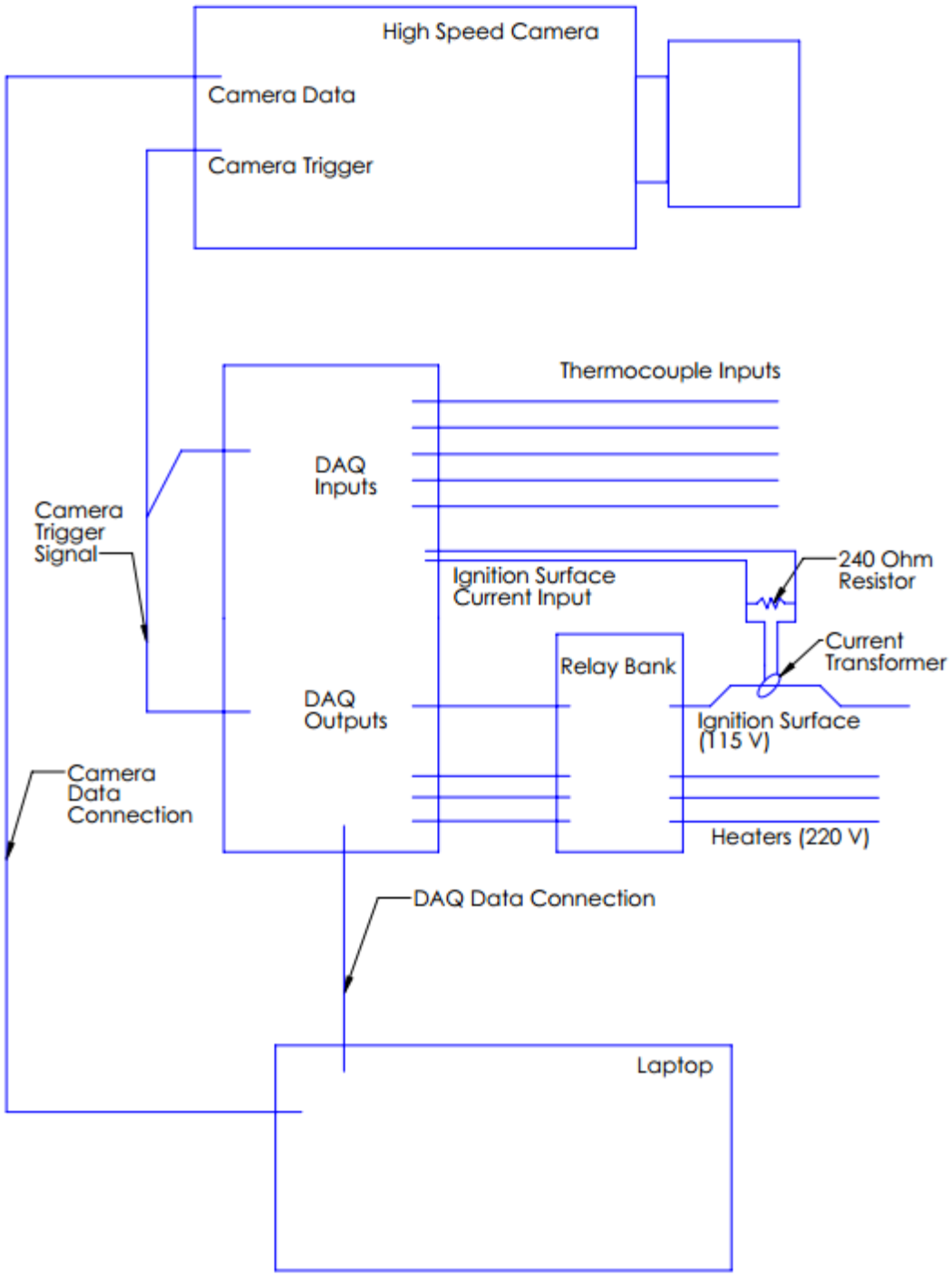

Figure 3.6: Diagram of the system

CHAPTER 4: RESULTS AND DISCUSSION

This chapter discusses the ignition properties of SME and CME blends with Jet A fuel at different equivalence ratios. In particular, results from Jet A and SME blend and Jet A and CME blend will be compared between 0%, 25%, 50%, 75%, and 100% concentration of SME and of CME, respectively. In each blend, the ignition properties including ignition temperature, ignition energy, ignition delay, power supplied to ignitor and the flame front velocities are presented and discussed.

4.1. Setup Calibration

4.1.1. Ignitor Temperature Calibration

The ignitor temperature was not measured directly; it was determined by sending a current through it and developing a relationship between the two parameters (Spens, 2017). Figure 4.1 shows the plot of current as a function of temperature, which is a nonlinear relationship. As the temperature increased from 20°C to 700°C, the current increased from 1.5 A to 5.5 A. However, as the temperature continued to rise to 1200°C from 700°C, the current dropped from 5.5 A to 4.5 A. This behavior could be explained due to the non-linear dependence of resistance of the ignitor on temperature.

Figure 4.2 and Figure 4.3 shows the relationship between current and temperature. The two figures represent the temperature in two scenarios: when the current increases with time and when the current decreases with time. The two best-fit polynomials were applied to the plots to obtain an equation for the temperature as a function of current. These are equation 3.5 and 3.6 in chapter 3. The R squared values for the two fit curves

were found at 0.995 and 0.914 respectively, indicating that these equations were a good fit to the plots.

Figure 4.4 presents the linear relationship of the temperature of the ignitor over time. The average rate of increase of temperature with respect to time was 110 K/s

4.1.2. Filling Duration

To calculate the time taken for the air-fuel mixture to fill up the chamber, Jet A was tested at equivalence of 1.00 with filling time varying from 30 to 120 seconds at 30 second interval. The result collected by Spens (2016) showed that average adjusted ignition energy was nearly constant for each filling time ranging between 269 J and 286 J. To provide an adequate duration of time for temperature and flowrate stabilization, as well as prerecording of the high speed camera, a filling time of 60 seconds was selected for the experiments.

4.1.3. Airflow Rates

Under the same conditions in filling time trial, Jet A was tested to determine the volumetric airflow rate to fill up the combustion chamber. An airflow rate of 24.0 L/min was used in place of 30.3 L/min which was used previously. From Spens (2016), the adjusted ignition energy was ranging from 202 J to 316 J, and averaged around 263 J. Comparing adjusted ignition energy between 24.0 L/min and 30.3 L/min, the lower airflow rate demonstrated a wider variation than that of the higher flowrate. There was no certain explanation for this variation; however the lower flow rate may have resulted in a less well-mixed fuel vapor/ air mixture, resulting in significant local equivalence ratio variations in the chamber. Thus, the filling airflow rates of 30.3 L/min were chosen due

to the smaller variation in ignition energy values, leading to more consistent results and less uncertainty in the measurements.

4.2. Results and Discussion

4.2.1. General observations

Figures 4.5 and 4.6 shows the comparison of the flames from Jet A, SME, their blends, and Jet A, CME, their blends, respectively, at an equivalence ratio of 1.40. The difference in brightness between the flames were insignificant. Figure 4.7 through Figure 4.12 displays the images captured by the high-speed camera of Jet A, SME, CME and their blends at various equivalence ratios. From these images, it was observed that the flames between the equivalence ratios of 1.30 and 1.50 were the brightest. At equivalence ratios of 0.75 and 2.00, the flames were extremely dim and propagated slower than flames at other equivalence ratios. As the equivalence ratio increased, the shape of the flame also showed a gradual change from the oval shape to a bell shape.

Figures 4.13 through 4.15 show the images captured by the high speed camera for the blends of Jet A and SME at an equivalence ratio of 1.40. The flame propagated outward from the ignitor. It was observed that the upper flame was moving at a significantly higher velocity than the lower flame. This behavior could be explained due to the buoyancy effect caused by high temperature inside the combustion chamber.

After every trial run, a brown deposit was found on the inside surface of the glass window. Figures 4.16 to 4.19 show the deposit buildup for the CME blends after each trial, where all nine equivalence ratios were tested. As the CME concentration increased, the deposit became clearer and thicker on the window surface. These types of deposits

were not noticed during Jet A trials (Spens, 2017). Biofuels have the tendency to produce more solid deposit during combustion, similar to the observations of Agarwal (2007), who documented significant deposits when biofuels were used in engines.

4.2.2. Jet A – SME Blends

4.2.2.1. Power to ignitor

Figures 4.20 to 4.22 display the power supplied to the ignitor as a function of time right before the ignition of Jet A and SME blends at three different equivalence ratios of 0.75, 1.00 and 1.30. The time in these plots indicated the time interval for ignition, meaning that the right end data points of the plots marked the point of ignition, which corresponded to the time interval for ignition plots discussed in the next few sections. By sending a current passage through the ignitor, the power was generated corresponding to the rise in temperature of the ignitor. During the time interval for ignition, the power increased and then flattened out as it approached the ignition point for all the fuels. It could be explained that as it got closer to the ignition point, the mixture temperature became higher, thus the heat transfer occurred between the ignitor and the environment reduced, leading to a drop in the power supply. This was similar to the ignitor temperature calibration discussed in section 4.1.1 since the current and temperature of the ignitor was closely related. It was discussed in Chapter 3 that the integral of power supplied to the ignitor over time (Equation 3.1) resulted in the energy of the ignition, which was the area under the curve in these plots. For the same time instance, Jet A displayed a slightly higher power supply comparing to the blends while pure SME showed a lower value than blends. On average, the power increased from 350 W to 650 W for tested fuels.

4.2.2.2. Ignition temperature

The ignition temperature, which is calculated by the current through ignitor, of all the blends is plotted in Figure 4.23 for SME blends at varying equivalence ratios. Generally, the ignition temperature slightly decreased from 700°C to 600°C with increasing equivalence ratio from 0.75 to 2.00. The uncertainty for ignition temperature measurements was ±34.7°C. In particular, at equivalence ratio of 1.00, Jet A and SME had an ignition temperature of around 685°C whereas their blends had a slightly lower ignition temperature of 660°C. The lack of dependence of ignition temperature on equivalence ratio was mentioned in studies by Kutcha et al. (1965), Kuchta and Cato (1966), and Boettcher (2012). Zabetakis et al. (1954) and Kutcha et al. (1965) noted the trend of increasing ignition temperature with increasing molecular weight of the fuel, yet, the results here was not in agreement with the two authors.

4.2.2.3. Time interval for ignition

Figure 4.24 presents variation in the time interval for ignition with respect to equivalence ratio of SME blends. This was the interval of time between the beginning of current passage through the ignitor and the appearance of a flame. Compared to the plots of power to ignitor, the ignition time interval on both plots might not be matching due to different data analyzing procedures. As current was passed through the ignitor, it got heated and heats the fuel/air mixture in the chamber. The heat was initially transferred primarily by conduction into the air-fuel mixture with no flow inside the chamber. The reaction rate is a highly non-linear function of temperature. As the fuel/air temperature got heated, the reaction rates increased until at some point when the energy generated exceeds the amount conducted away; this marks the generation of the flame front. The

time interval for ignition (the time between the appearance of the first flame front and the beginning of passage of current through the ignitor) was around 2.3 s at an equivalence ratio of 0.75. As the equivalence ratio increased (the mixture became more stoichiometric), reaction rates increased resulting in a decrease in the time of ignition. Specifically, time interval for ignition decreased from 2.3 s to 1.6 s for increasing equivalence ratio from 0.75 to 2.00 for all the blends. Generally, Jet A had the longest time interval, followed by SME blends. In other words, as the Jet A concentration decreased, the time interval for ignition also decreased. Uncertainty for the time interval for ignition averaged ±0.24 s.

4.2.2.4. Ignition energy

The measured ignition energy of SME blends is shown in Figure 4.25. The variation of measured ignition energy with equivalence ratio and fuel was in a similar manner to time interval for ignition. Jet A had the highest measured ignition energy, followed by the blends and then the pure SME. As the equivalence ratio increased, the measured ignition energy decreased from 1200J to 800J. This result was expected since a smaller time interval for ignition produced in a smaller range for integration in Equation 3.1 and lower ignition energy. The averaged uncertainty for measured ignition energy at 95% confidence was ±119.19 J. Because the ignitor was heated up at a constant rate, the time interval for ignition and measured ignition energy were coupled and depended on the initial temperature of the ignitor.

The adjusted ignition energy is plotted for Jet A, SME and their blends in Figure 4.26 as a function of equivalence ratio. The adjusted ignition energy was used to account for the energy lost through radiation. The behavior of adjusted ignition energy was

expected and similar to the measured ignition energy since the energy loss due to radiation was observed to decrease with increasing equivalence ratio as well. Specifically, the adjusted ignition energy decreased from around 1150J to 750J as the equivalence ratio increased from 0.75 to 2.00. Jet A had a slightly higher energy while pure SME had a slightly lower energy than the rest of the blends. The averaged uncertainty for a confidence value of 95% was ±78 J for 25J75S, ±116 J for 50J50S, and ±64 J for 75J25S. The laminar flame velocity of SME is only slightly lower than that of diesel (14 % lower at an equivalence ratio of 1.1 and 10% lower at an equivalence ratio of 1.2) and comparable to that of Jet A (Gómez-Meyer, 2012). This indicates that the reaction rates of the two fuels at the same temperature are comparable, leading to comparable ignition energy values.

4.2.2.5. Lower flame velocity

The upper and lower flame velocities for pure SME at equivalence ratio of 1.30 is shown in Figure 4.27. Both velocities increasing with time suggested that the flames accelerated during the combustion. The difference between upper and lower flame velocities could be explained due to buoyancy effect, which would be thoroughly discussed later.

The lower flame velocity as a function of equivalence ratio for SME blends are presented in Figure 4.28. The velocity was calculated using images captured by the high-speed camera during the flame propagation period. The plots were parabola-shaped in a downward fashion. All the fuels peaked at an equivalence ratio of 1.40. The pure fuels seemed to have a lower peak velocity comparing to their blends. In particular, Jet A, and SME flames reached maximum velocity at around 3.2 m/s and 2.3 m/s at equivalence

ratio of 1.40, respectively, whereas their blends went at some values in between. Uncertainty for lower flame velocities was averaged at ±0.80 m/s.

A study by Gómez-Meyer et al. (2012) measured the laminar flame velocities of diesel as well as SME and CME for equivalence ratios of 1.0, 1.1, and 1.2. Both SME and CME flame velocities peaked at an equivalence ratio of 1.1 with the values of 1.07 m/s and 1.10 m/s, respectively. Comparing these values to those of current study, a difference can be noted. This was due to of the larger temperature in the current study and the flame velocity temperature dependence of $T^{1.5}$, increasing the reaction rate and flame front velocity.

4.2.2.6. Upper flame velocity

The plots of average upper flame front velocities were shown in Figure 4.29. The upper flame front velocities were parabolic in nature similar to the lower flame velocity case, reaching a peak of equivalence ratio of 1.40. Jet A had a maximum flame velocity of around 6.5 m/s where the its blends with SME displayed a slightly lower velocity, around 5 m/s to 6 m/s, and pure SME had the lower upper flame velocity of around 4.2 m/s. The uncertainty was averaged at ±0.87 m/s for the fuels tested.

It can be noted that the upper flame front velocities were significantly higher than the lower flame front velocities. This was due to the significant buoyancy effects, caused by high temperature flame which caused a decrease in density of the combustion products. The density of air at 648 K is 0.55 kg/m^3, whereas at 2200 K (flame temperature), it is 0.16 kg/m^3. Thus, the upper flame front is subject to a significant buoyant acceleration; buoyancy acts opposite to the direction of flame propagation for the

lower flame front causing the corresponding values to be smaller than those measured for the upper flame front.

4.2.3. Jet A – CME Blends

Generally, since CME fuel possesses similar properties as fuel, thus, ignition behaviors of its blends with Jet A were also found to be insignificantly different compared to those of SME blends.

4.2.3.1. Power to ignitor

The power supplied to the ignitor of CME blends at three different equivalence ratios is plotted from Figure 4.30 to Figure 4.32. Similar to SME blends, the power increased linearly with respect to time interval, which again was the time it took for the ignition to occur after the current was passed through the ignitor. Power at every instance supplied to the blends and the pure CME was found to be very close to each other. Even though the time interval for CME and the blends was longer, which indicated a longer power supply to the ignitor, the ignition energy of those fuels was still lower than that of Jet A.

This was due to the fact that the Jet A had a slightly higher power supply than the rest of the fuels. At the beginning, the power was supplied to the ignitor at around 350 W and increased to 620 W at the time of ignition.

4.2.3.2. Ignition temperature

Figure 4.33 shows the ignition temperature as a function of equivalence ratio of the CME blends. The ignition temperature was found to decrease from 700°C to 600°C with increasing equivalence ratio from 0.75 to 2.00, which was in the same range as SME blends. The uncertainty for ignition temperature measurements was found at ±31.3°C.

4.2.3.3. Time interval for ignition

Figure 4.34 presents variation in the time interval for ignition with respect to equivalence ratio of the CME blends. The time interval for ignition decreased from 2.5 s to 1.7 s as the equivalence ratio increased from 0.75 to 2.00. The blends were found to have a slightly higher time interval than Jet A and CME. This suggested that blends of biofuel behaved non-monotonically in terms of ignition properties. The averaged uncertainty at 95% confidence was found at around ± 0.27 s.

4.2.3.4. Ignition energy

The measured ignition energy of the CME blends is shown in Figure 4.35. The blends had the highest measured ignition energy, followed by the Jet A and then the pure CME. This, again, proved the non-monotonic behaviors of the biofuel blends. As the equivalence ratio increased, the measured ignition energy decreased from the average of 1300 J to 870 J. The averaged uncertainty for measured ignition energy at 95% confidence was ±115 J.

Figure 4.36 shows the adjusted measured ignition energy of the CME blends, which acted in a similar manner to the measured ignition energy. Due to loss to radiation, the adjusted ignition energy decreased from around 1200 J to 830 J as the equivalence ratio increased. The averaged uncertainty for a confidence value of 95% was ±86 J for 25J75C, ± 55J for 50J50C, and ±102 J for 75J25C

4.2.3.5. Lower flame velocity

The lower flame velocity as a function of equivalence ratio for CME blends are presented in Figure 4.36. Similar to SME blends, the plots were parabola-shaped in a downward fashion with the peak velocity at an equivalence ratio of 1.40. CME and Jet A

flames reached a maximum velocity of around 3.4 m/s where their blends went as high as 3 m/s. The uncertainty was averaged at ±1.04 m/s for the fuel tested.

4.2.3.6. Upper flame velocity

The plots of average upper flame front velocities are shown in Figure 4.38. The upper flame front velocities reach a peak at equivalence ratio of 1.40. Similar to lower flame velocity, Jet A and CME had a slightly higher peak velocity than their blends, reaching maximum flame velocity of around 6.8 m/s where the its blends peaked around 5 m/s to 6 m/s. Uncertainty for lower flame velocities was averaged at ±0.88 m/s

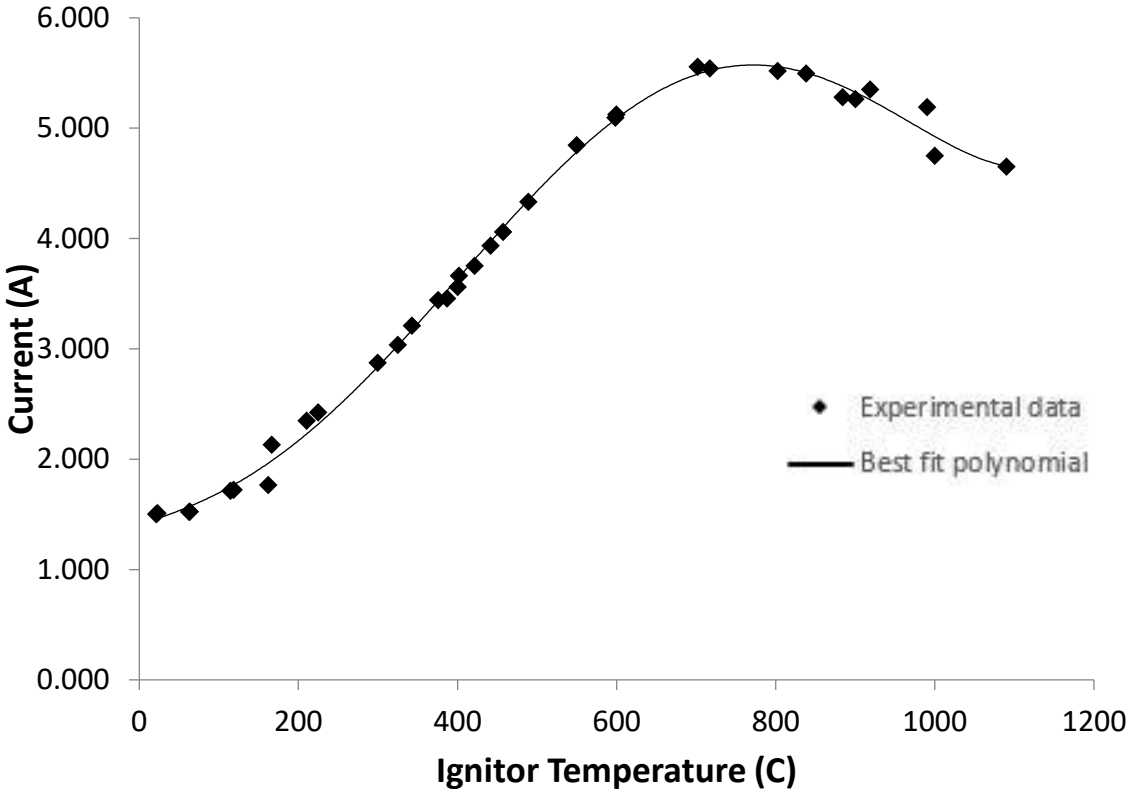

Figure 4.1: Ignitor current at various temperatures (Spens, 2017)

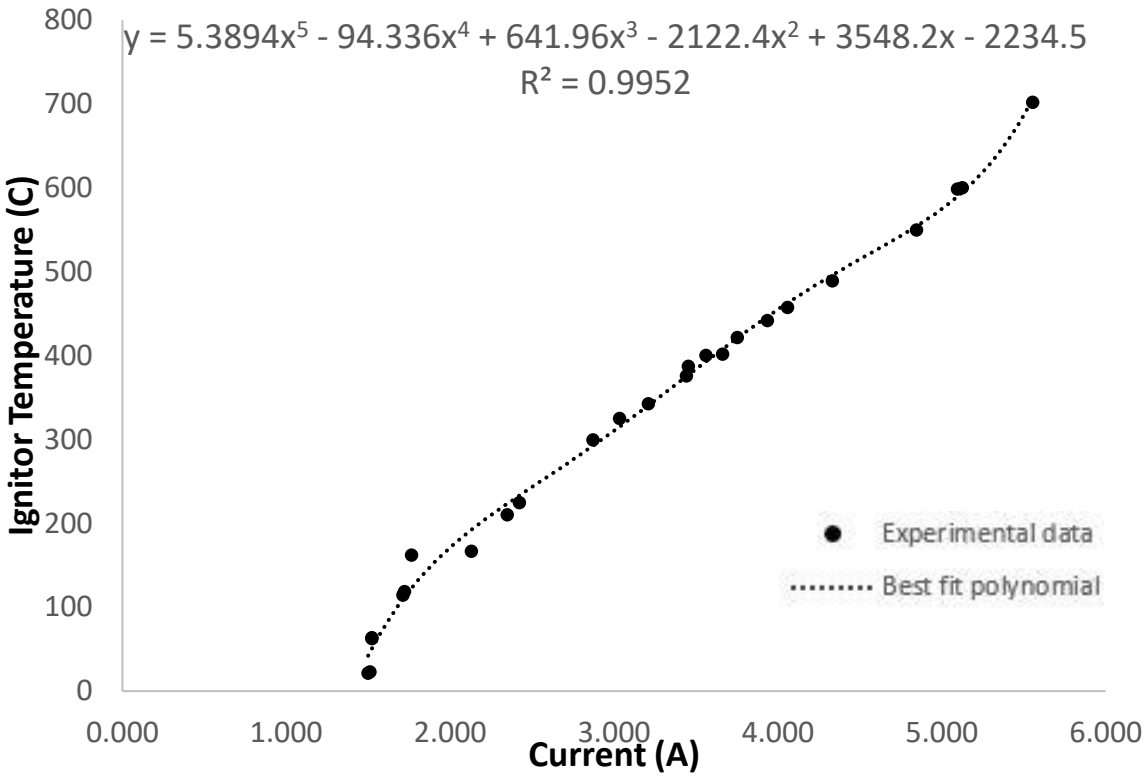

Figure 4.2: Ignitor temperatures as a function of current and increasing in current over time (Spens, 2017)

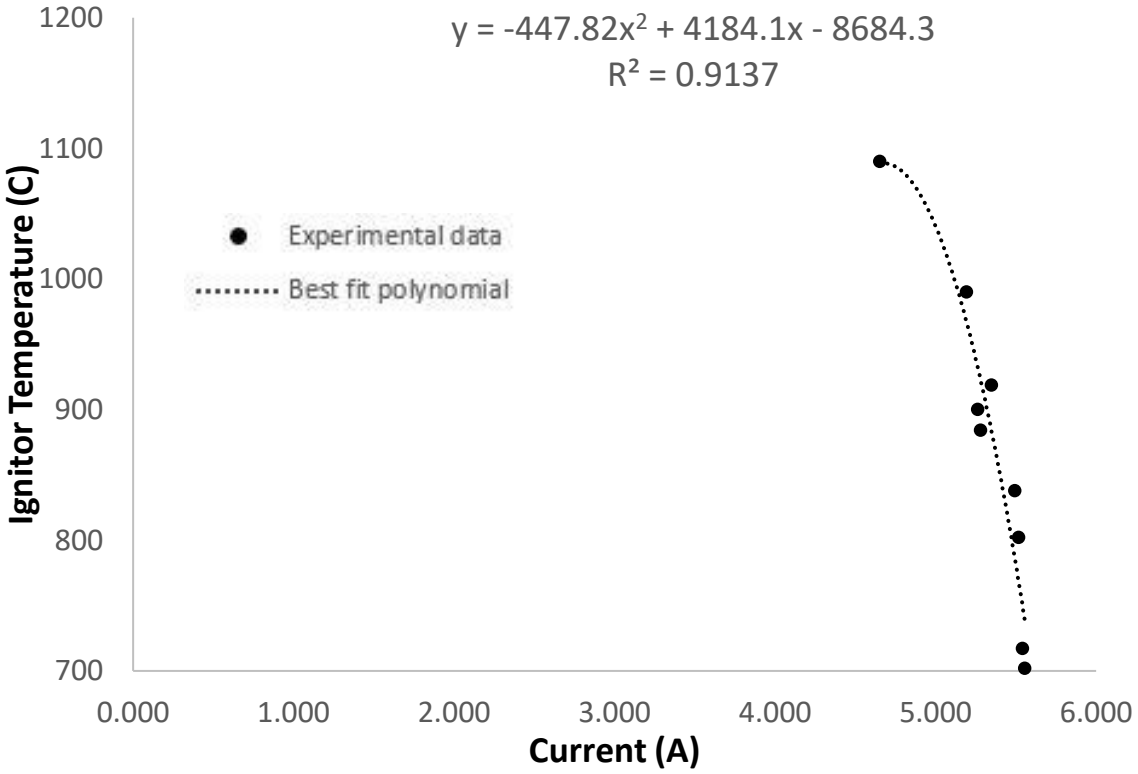

Figure 4.3: Ignitor temperatures as a function of current and decreasing in current with time (Spens, 2017)

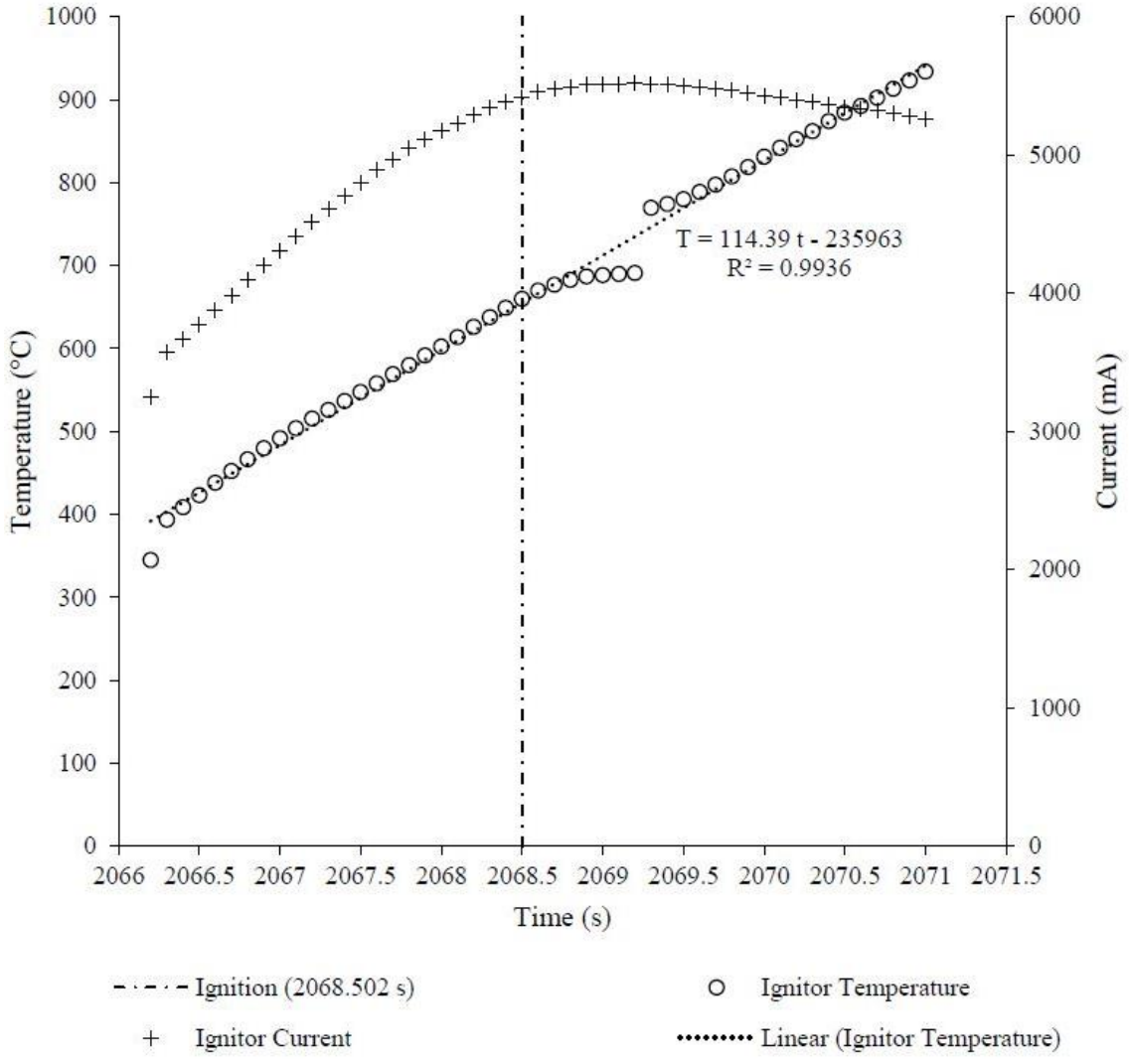

Figure 4.4: Ignitor temperature varying with time of Jet A at equivalence of 1.00 (Spens, 2017)

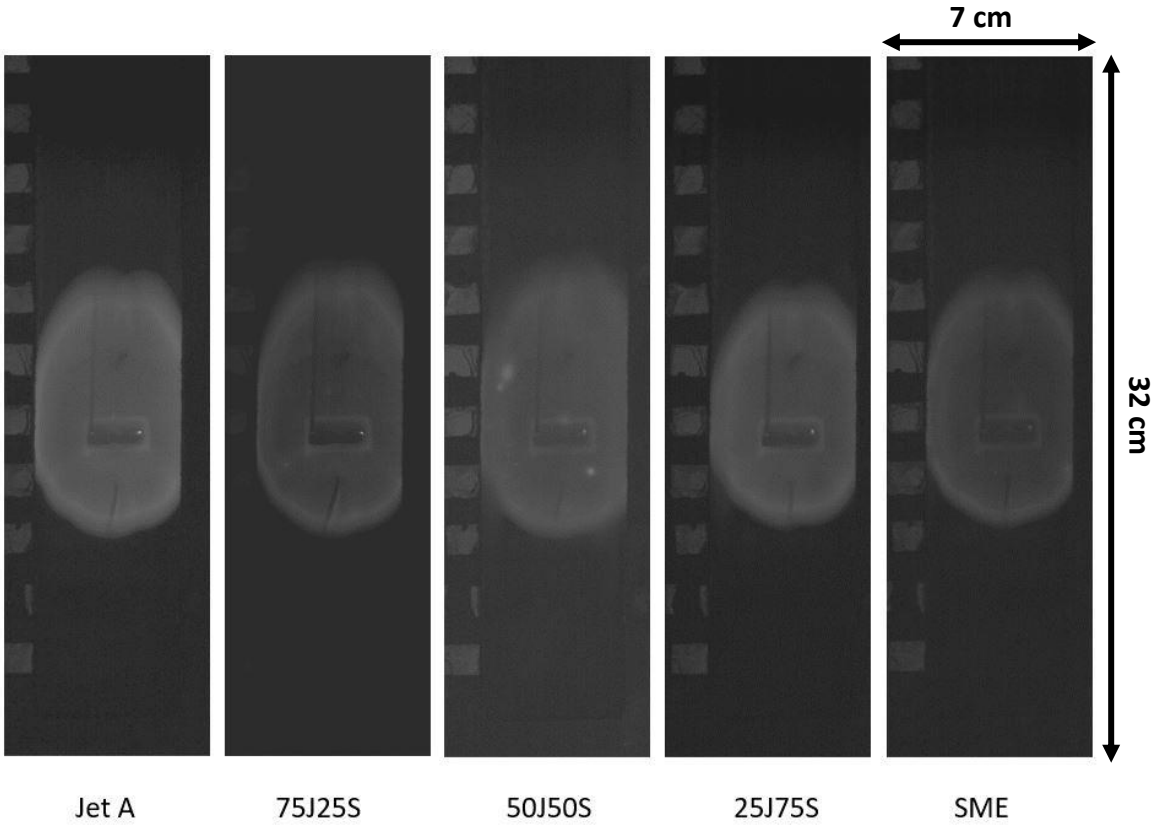

Figure 4.5: Typical flames of Jet A, SME and their blends at an equivalence ratio of 1.4 (0.012s after ignition)

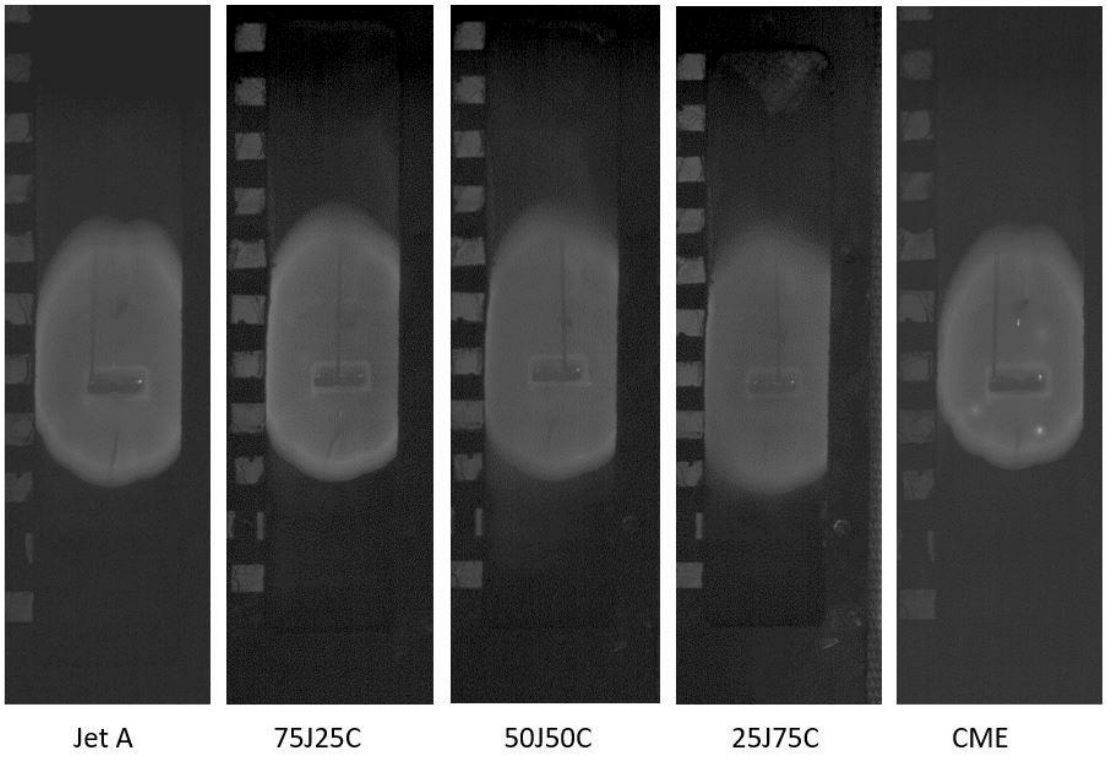

Figure 4.6: Typical flames of Jet A, CME and their blends at an equivalence ratio of 1.4 (0.012s after ignition)

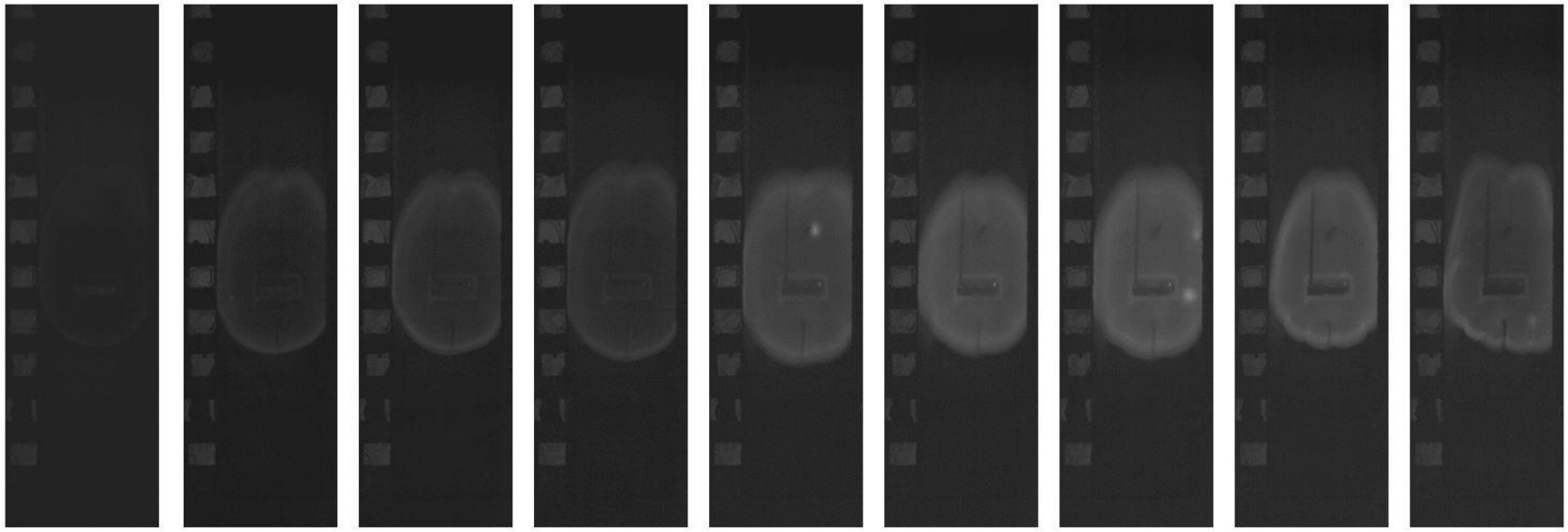

Figure 4.7: Images of 25J75S fuel at various equivalence ratios

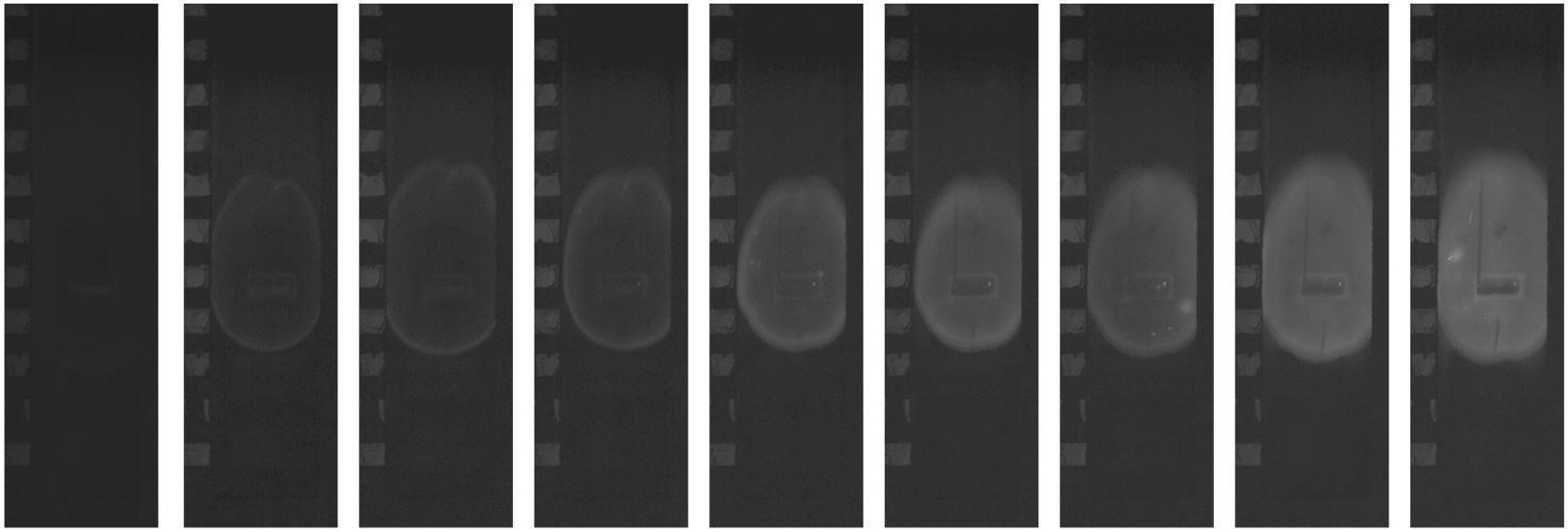

Figure 4.8: Images of 50J50S fuel at various equivalence ratios

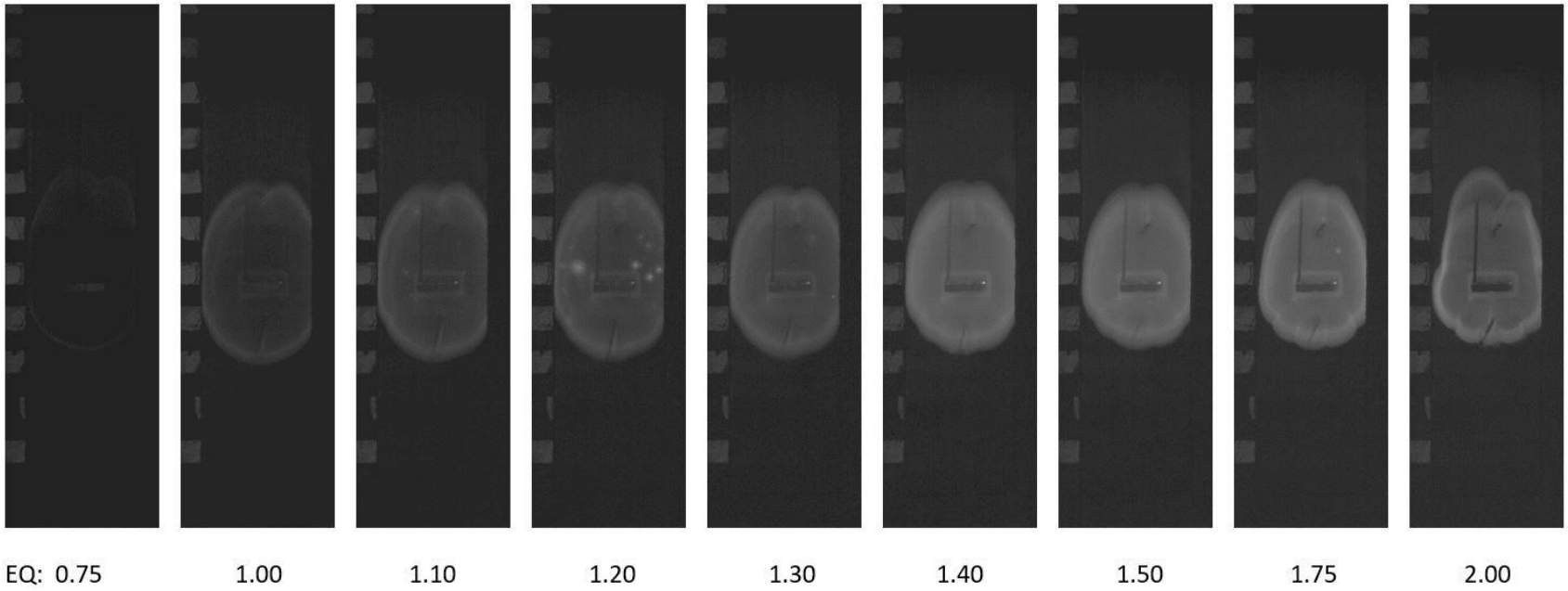

Figure 4.9: Images of 75J25S fuel at various equivalence ratios

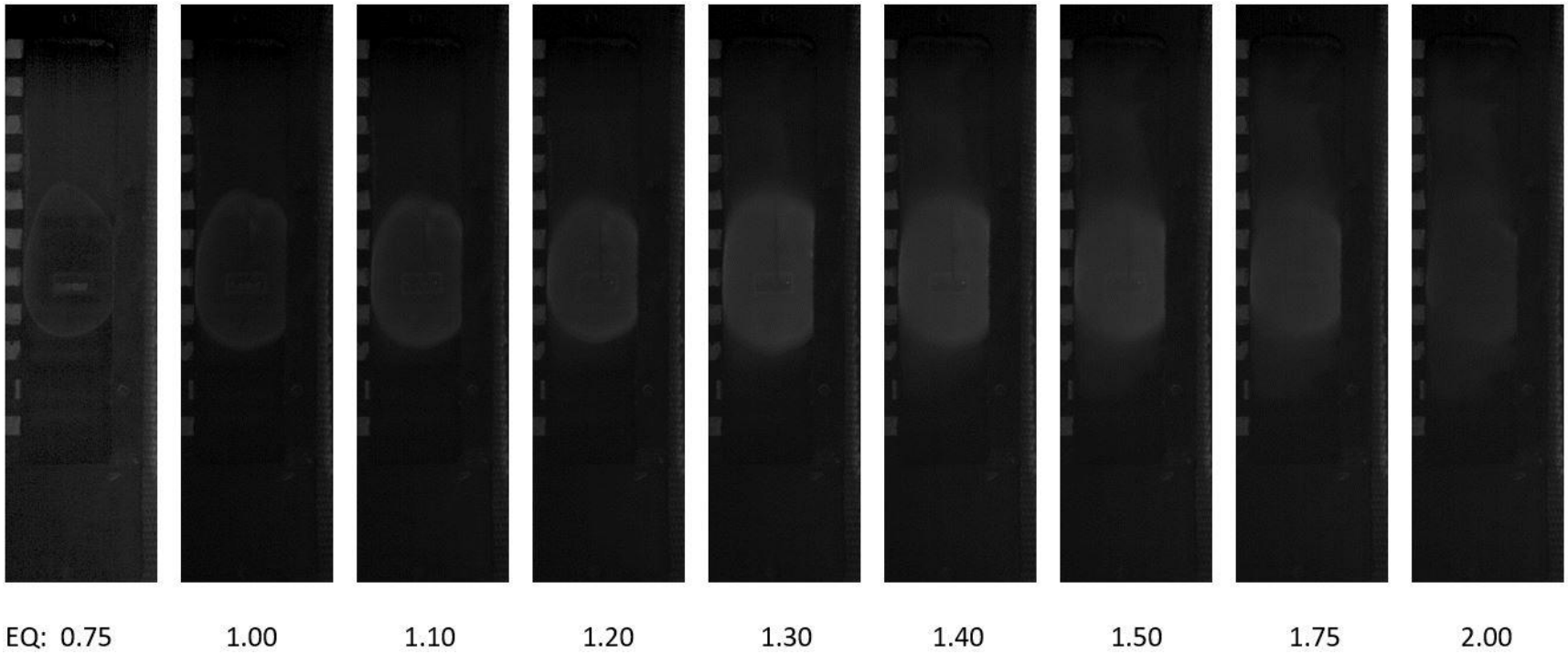

Figure 4.10: Images of 25J75C fuel at various equivalence ratios

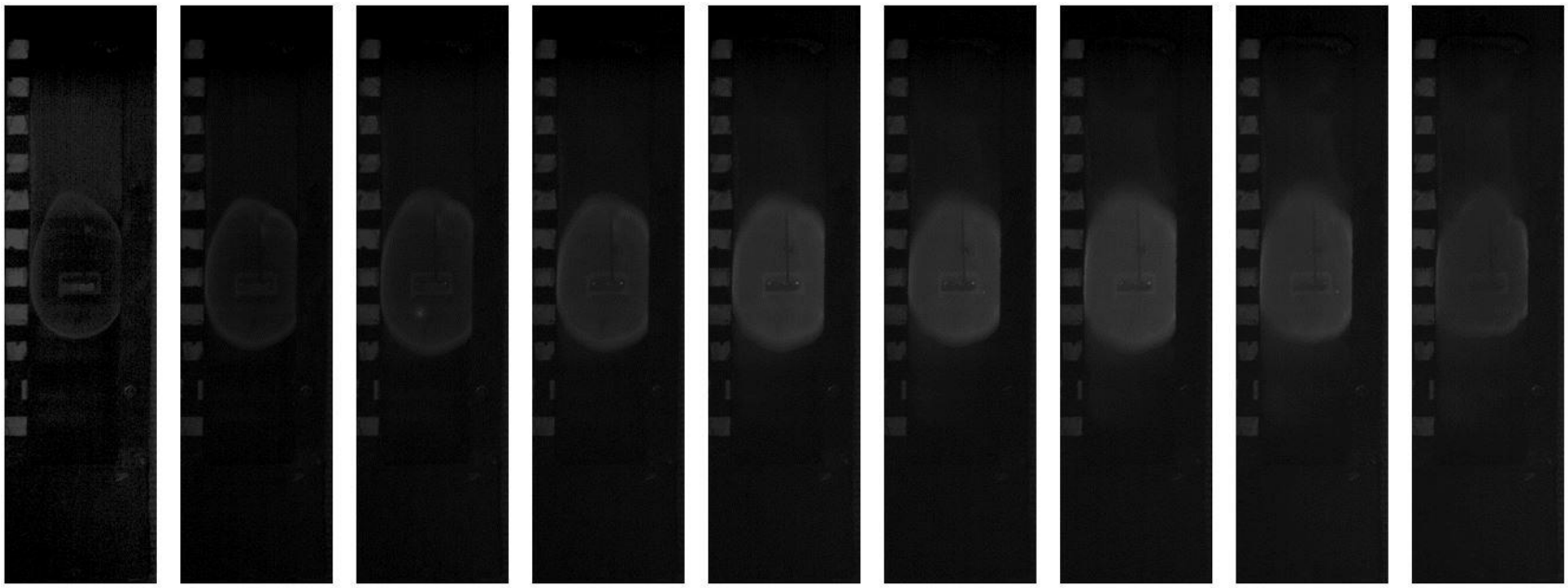

Figure 4.11: Images of 50J50C fuel at various equivalence ratios

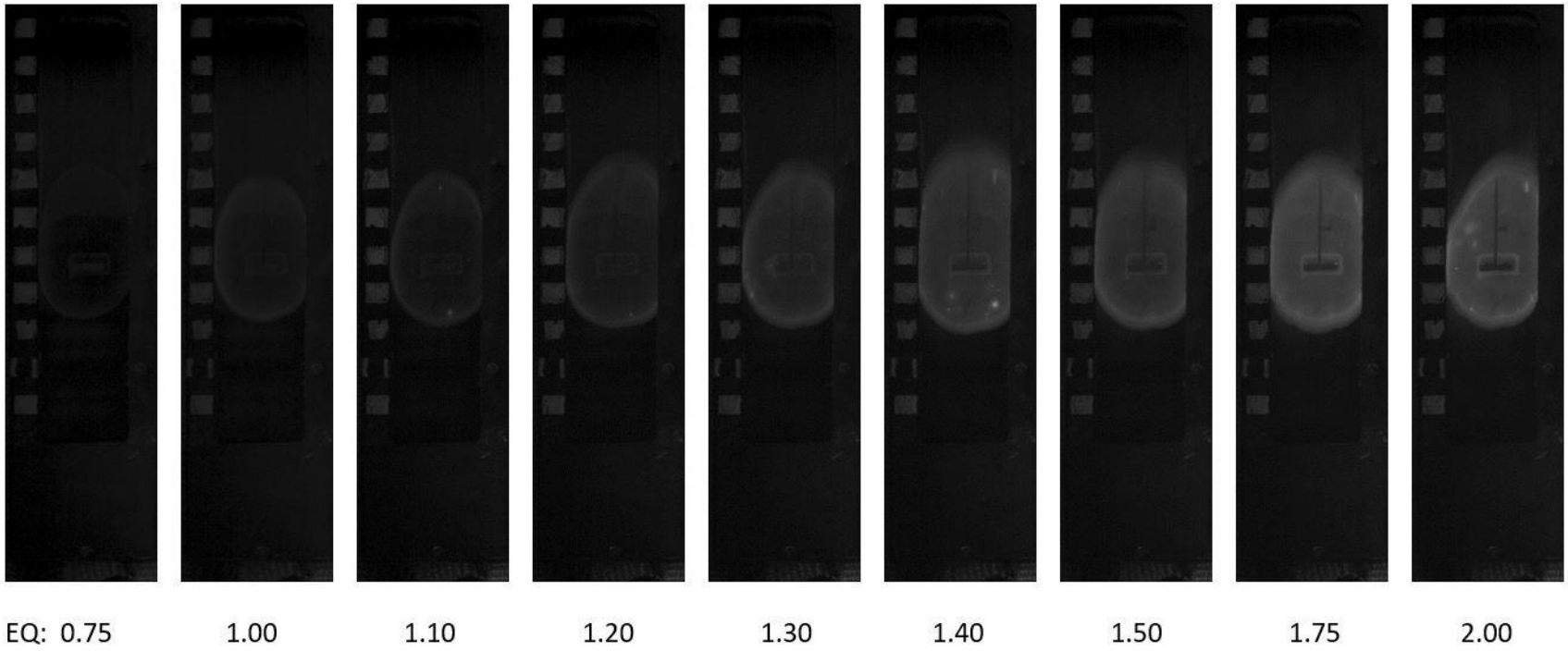

Figure 4.12: Images of 75J25C fuel at various equivalence ratios

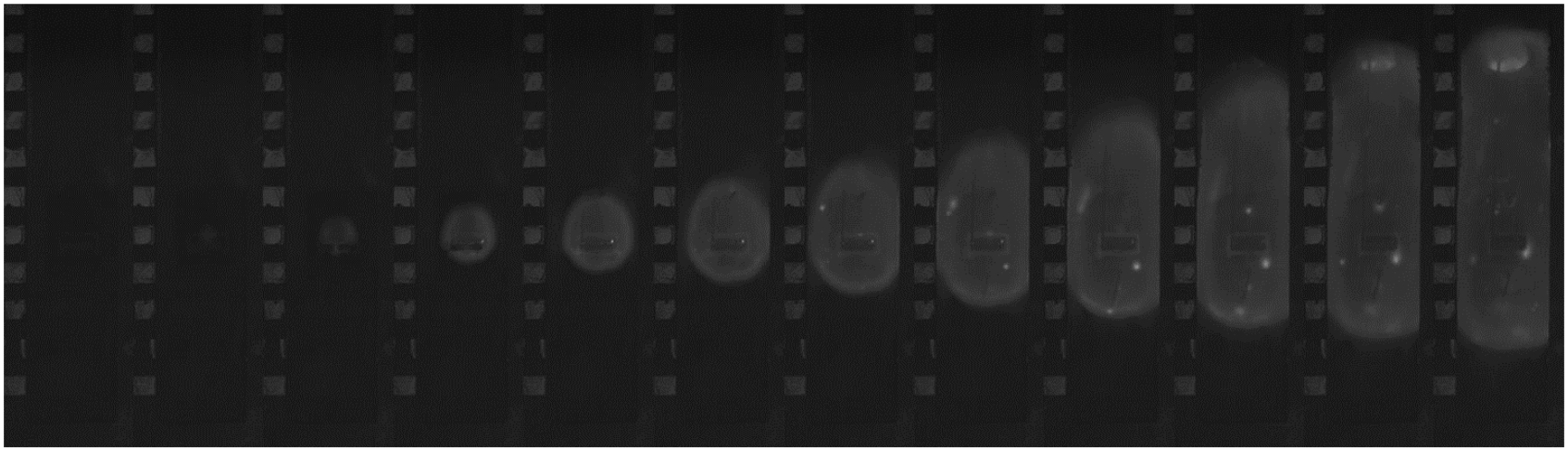

Figure 4.13: Typical flames of 75J25S fuel at equivalence of 1.40, each frame is 0.002s apart

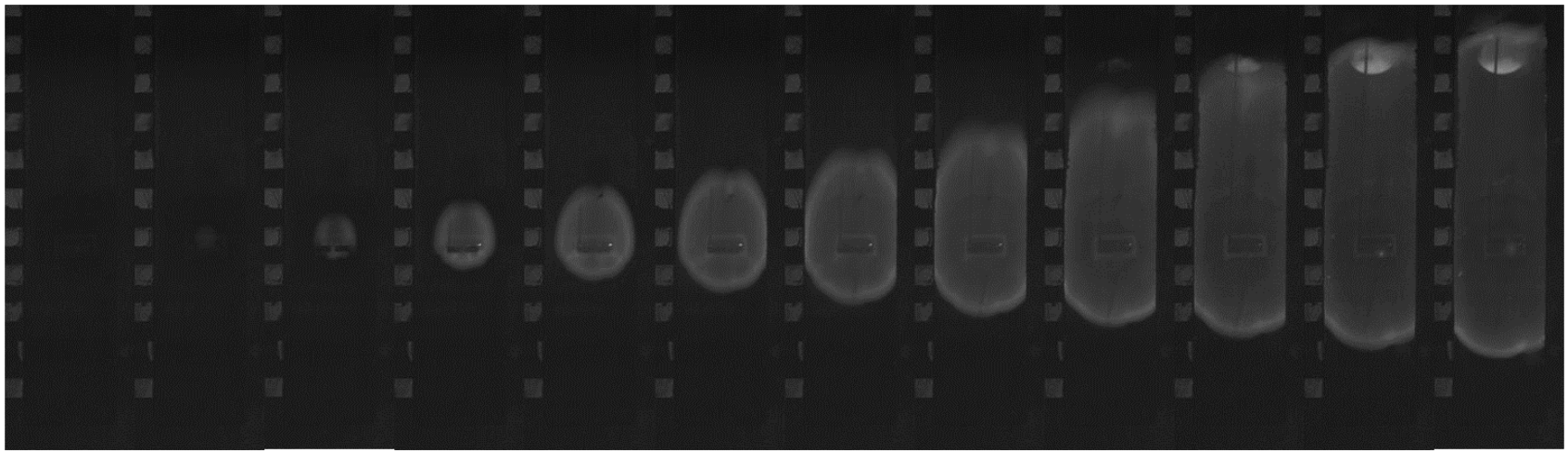

Figure 4.14: Typical flames of 50J50S fuel at equivalence of 1.40, each frame is 0.002s apart

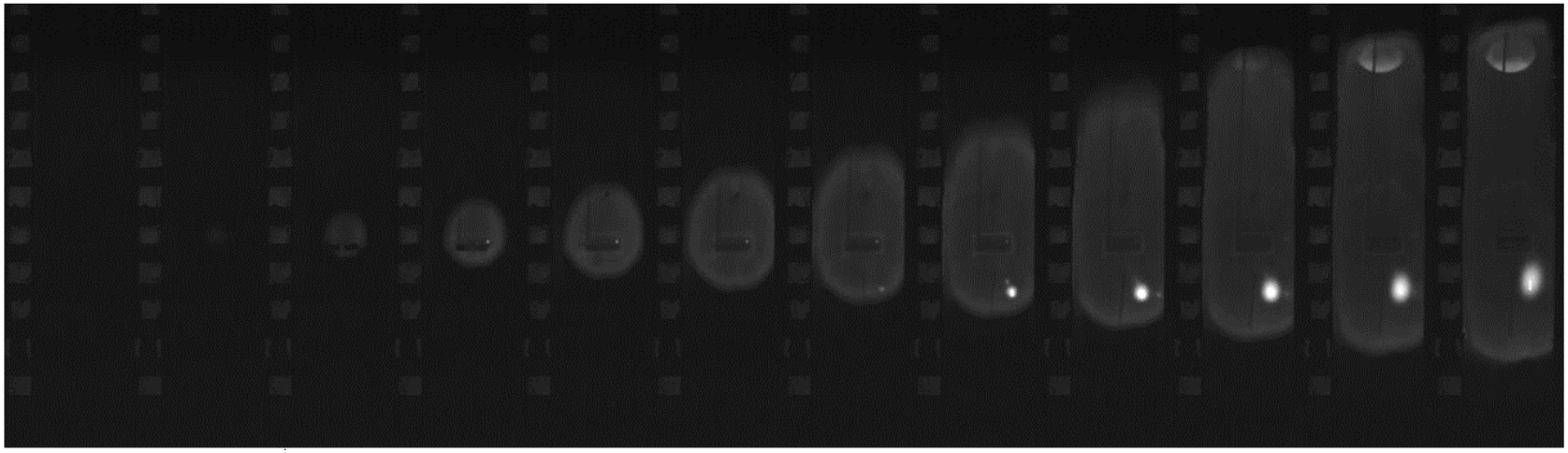

Figure 4.15: Typical flames of 25J75S fuel at equivalence of 1.40, each frame is 0.002s apart

Figure 4.16: Appearance of window glass of 75J25C fuel

Figure 4.17: Appearance of window glass of 50J50C fuel

Figure 4.18: Appearance of window glass of 25J75C fuel

Figure 4.19: Appearance of window glass of CME fuel

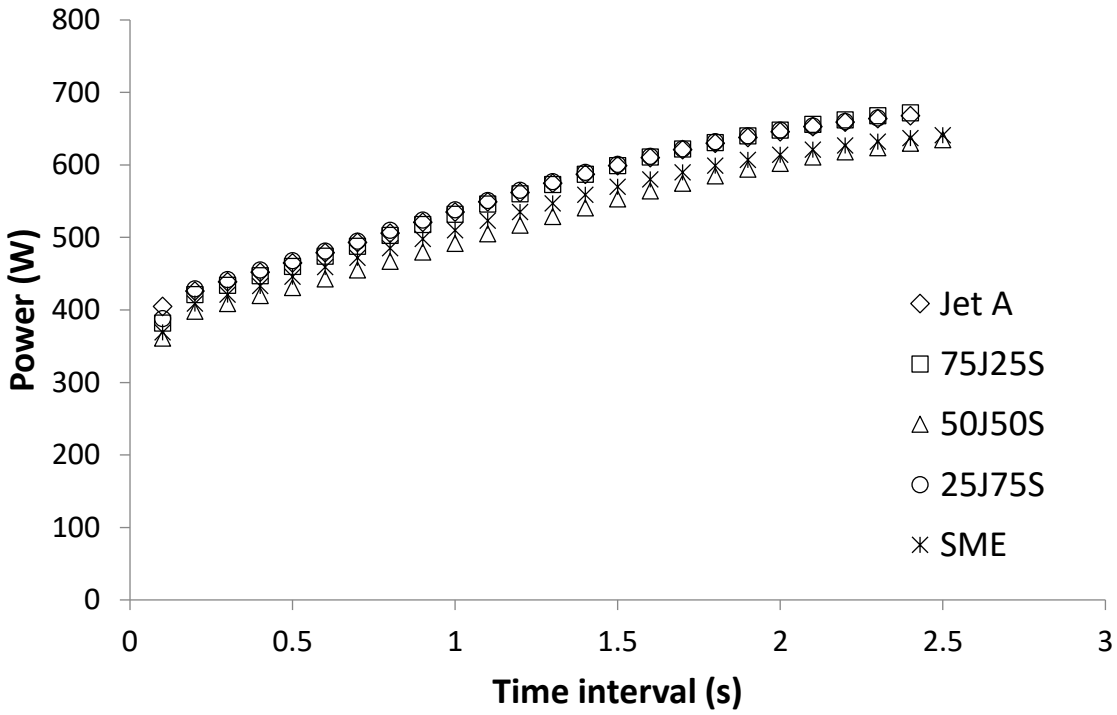

Figure 4.20: Power to the ignitor as a function of time of Jet A – SME Blends at equivalence ratio of 0.75

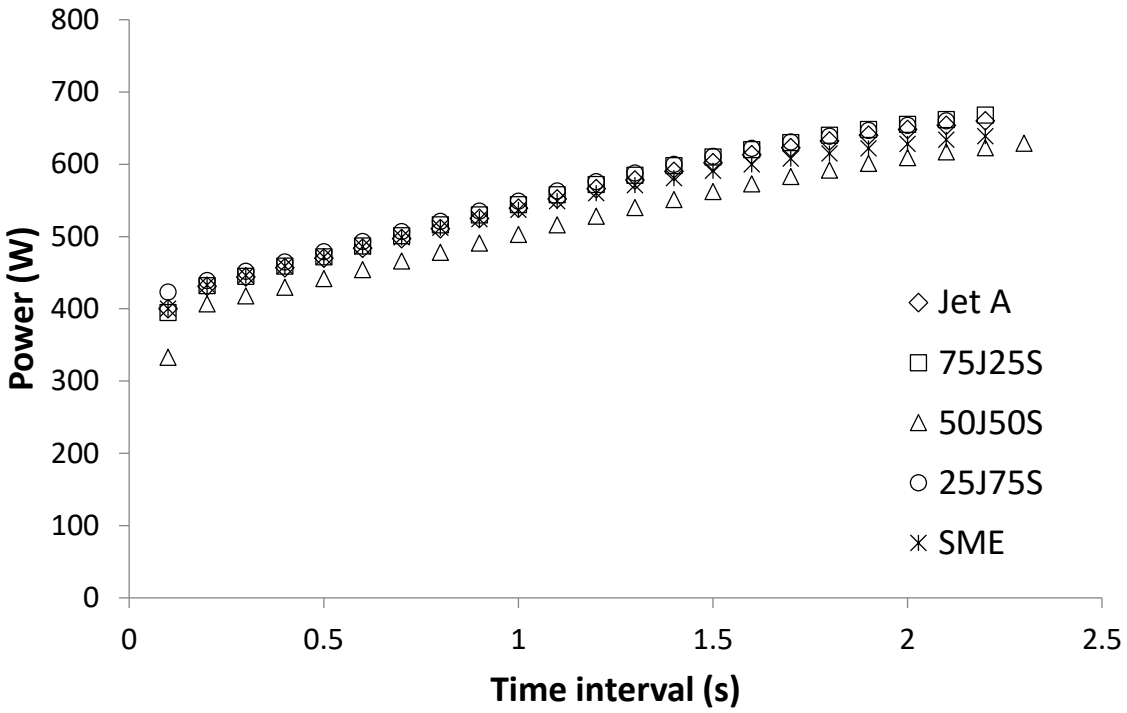

Figure 4.21: Power to the ignitor as a function of time of Jet A – SME Blends at equivalence ratio of 1.00

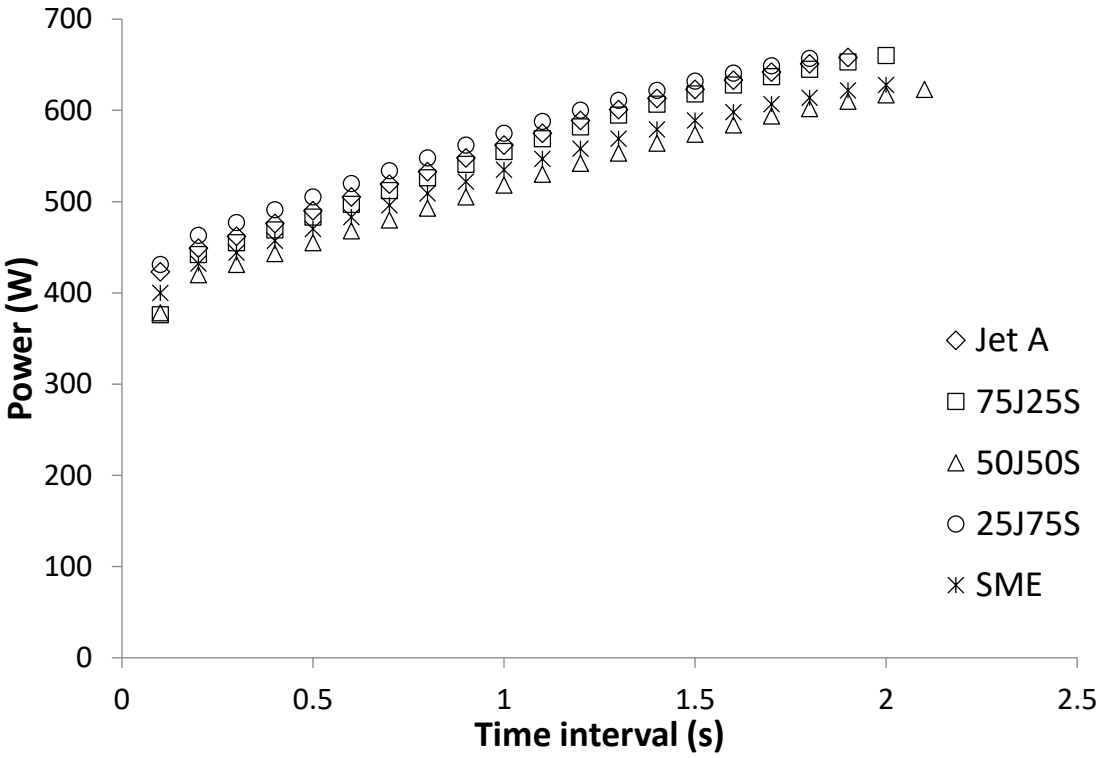

Figure 4.22: Power to the ignitor as a function of time of Jet A – SME Blends at equivalence ratio of 1.30

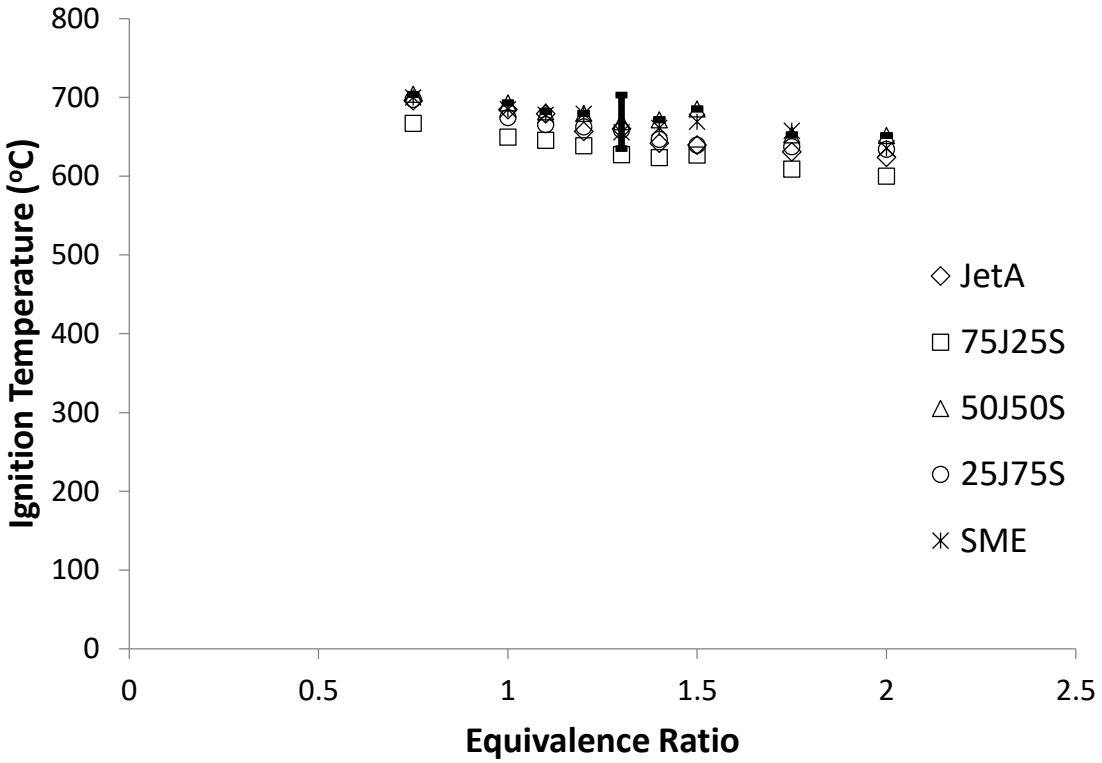

Figure 4.23: Ignition temperature at varying equivalence ratios of Jet A – SME Blends

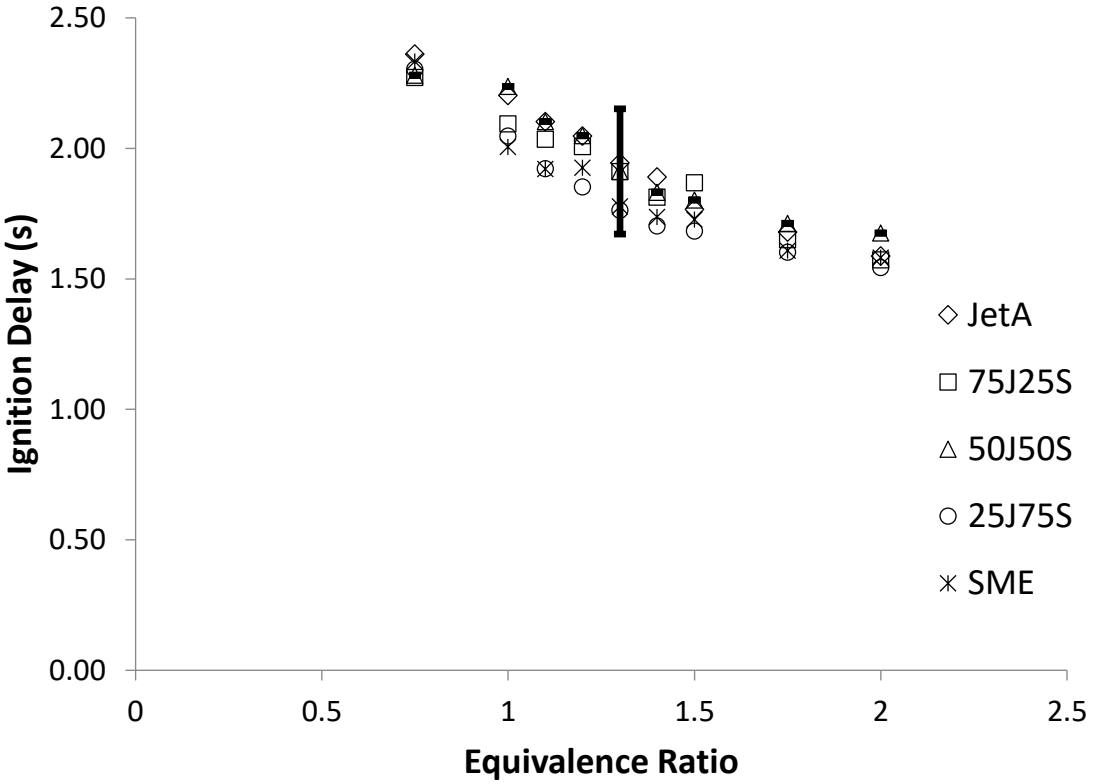

Figure 4.24: Time interval for ignition at varying equivalence ratios of Jet A – SME Blends

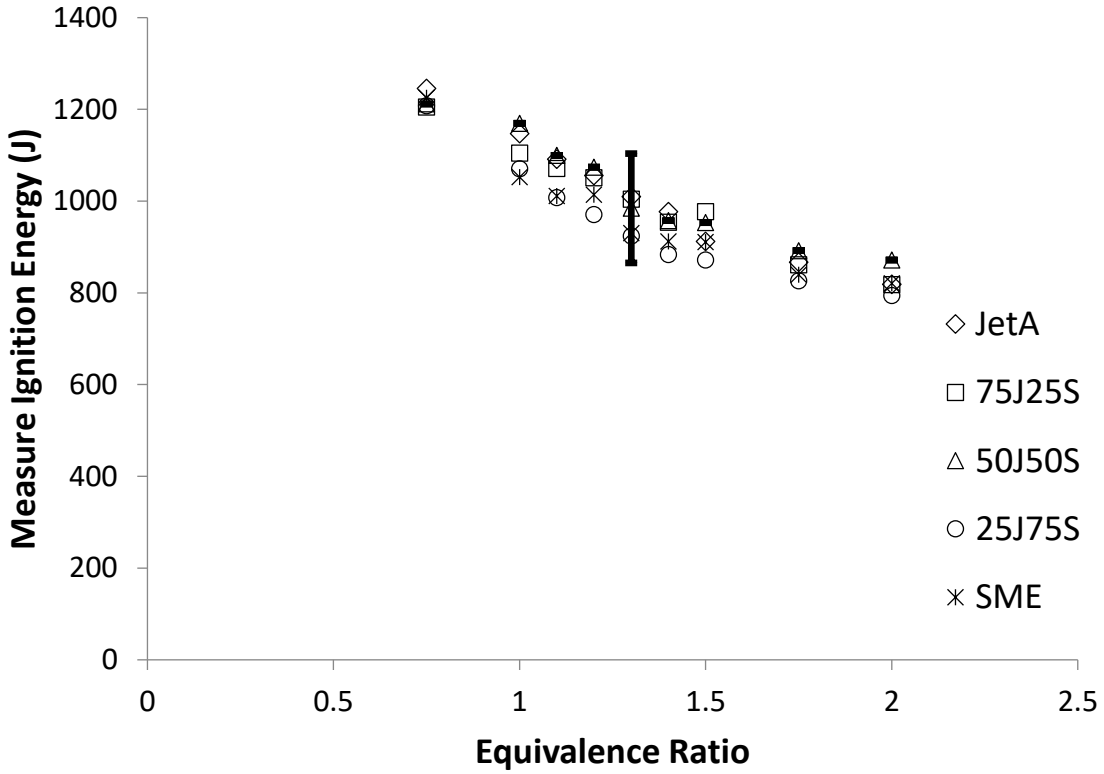

Figure 4.25: Measured ignition energy at varying equivalence ratios of Jet A – SME Blends

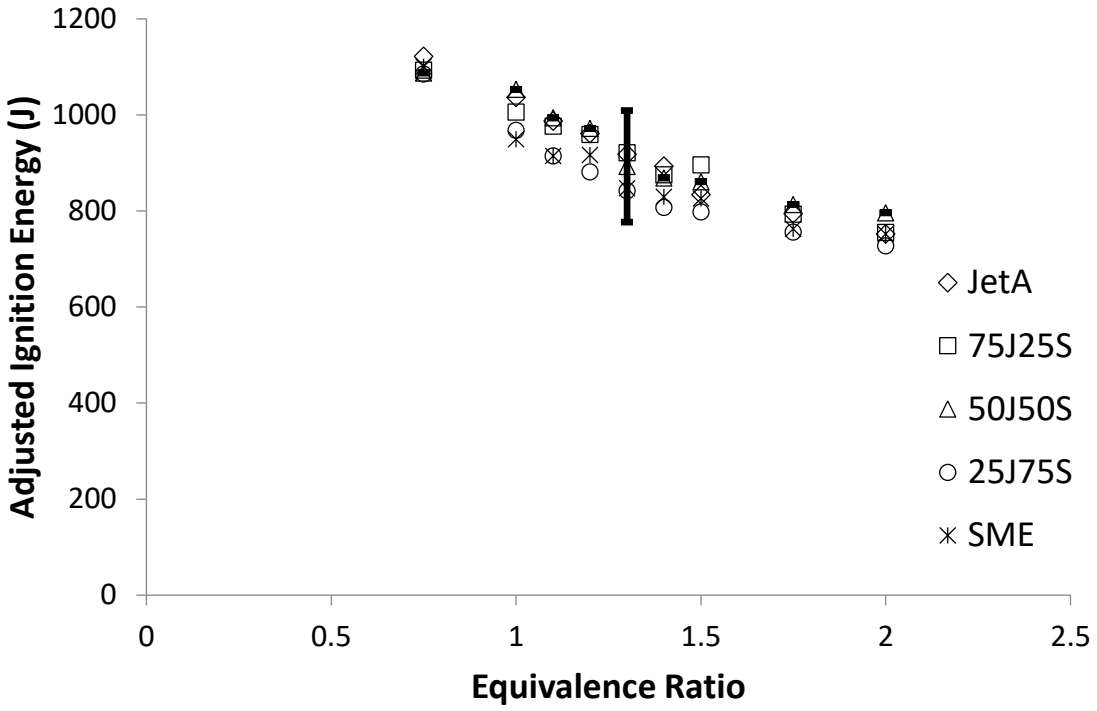

Figure 4.26: Adjusted ignition energy at varying equivalence ratios of Jet A – SME Blends

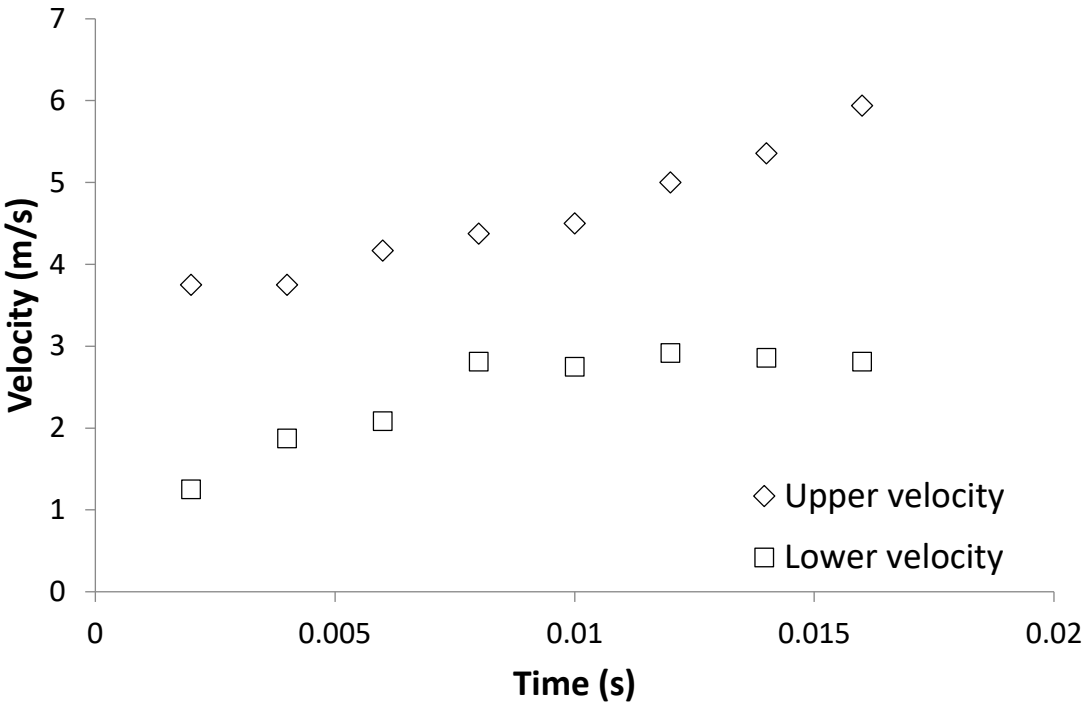

Figure 4.27: Flame velocities of pure SME at equivalence ratio of 1.30

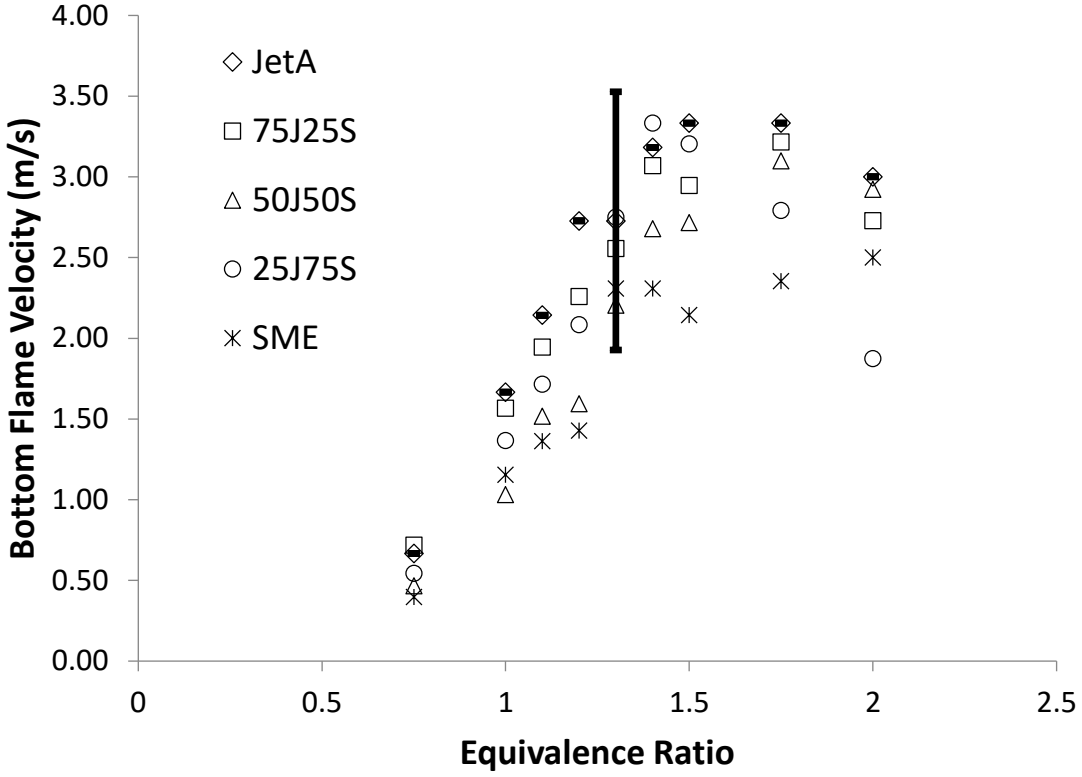

Figure 4.28: Lower flame velocity at varying equivalence ratios of Jet A – SME Blends

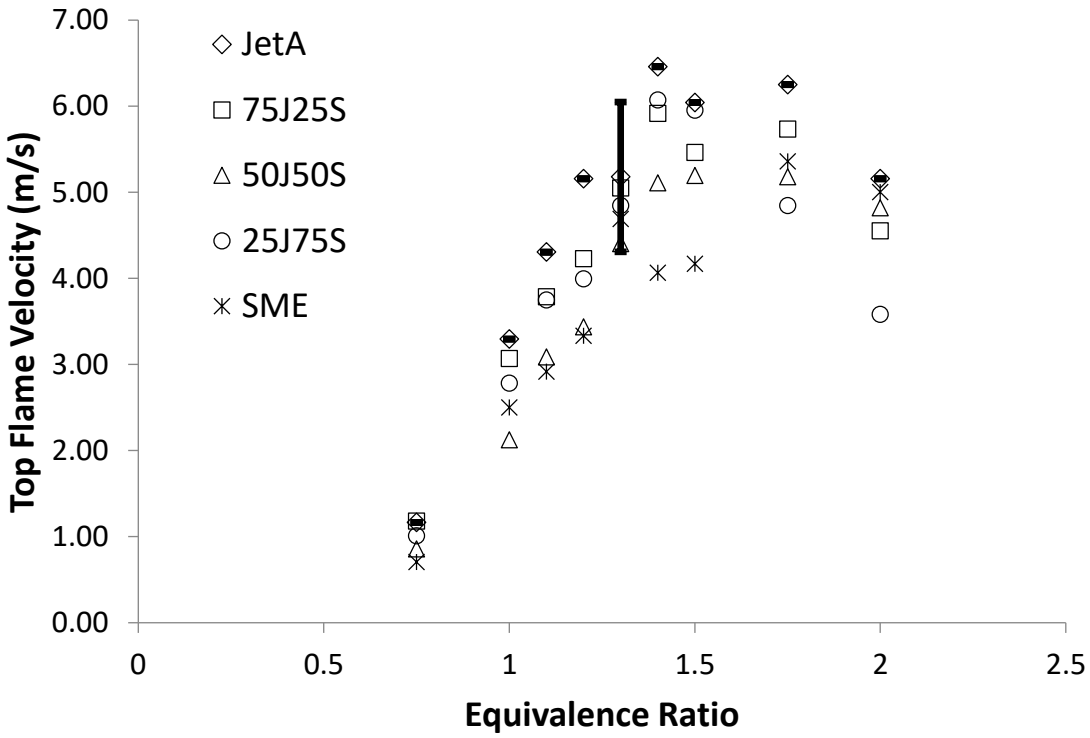

Figure 4.29: Upper flame velocity at varying equivalence ratios of Jet A – SME Blends

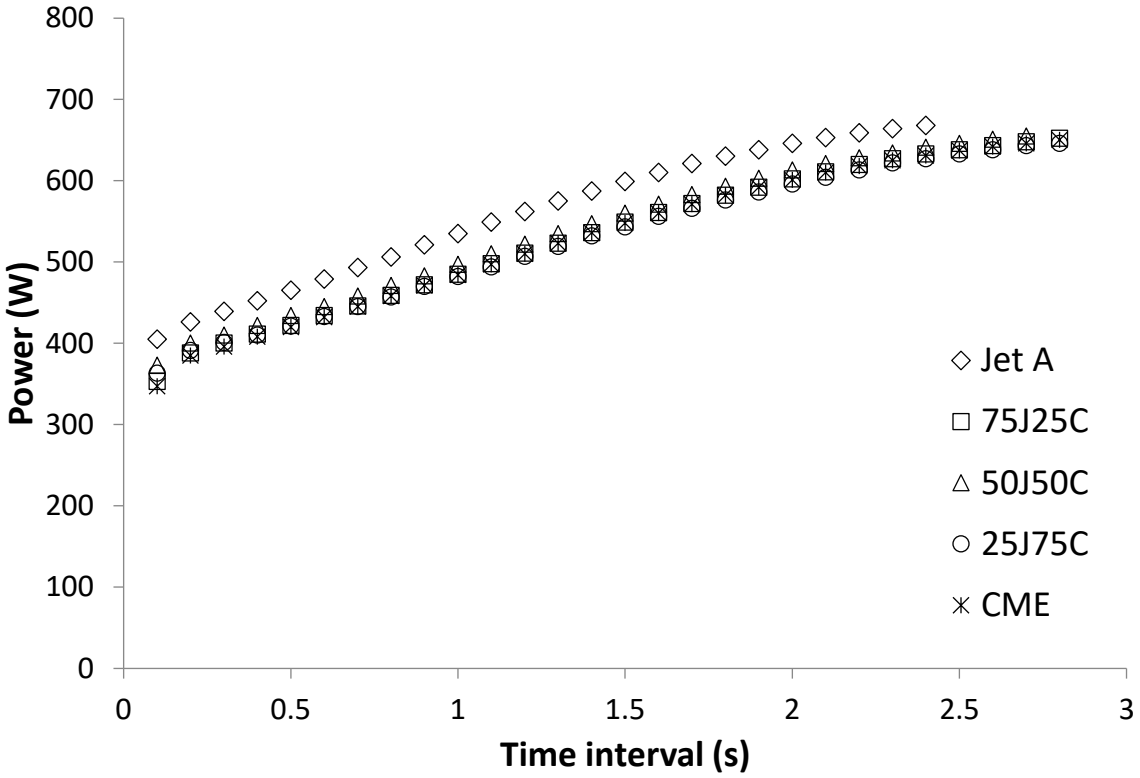

Figure 4.30: Power to the ignitor as a function of time of Jet A – CME Blends at equivalence ratio of 0.75

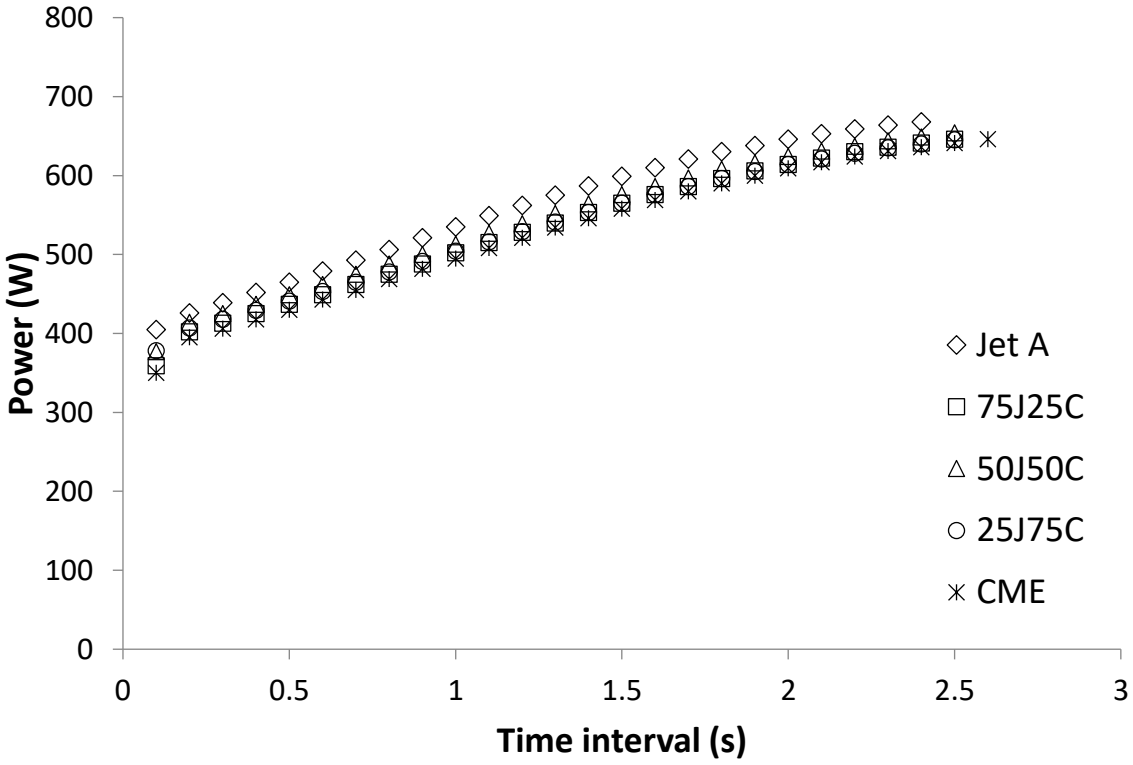

Figure 4.31: Power to the ignitor as a function of time of Jet A – CME Blends at equivalence ratio of 1.00

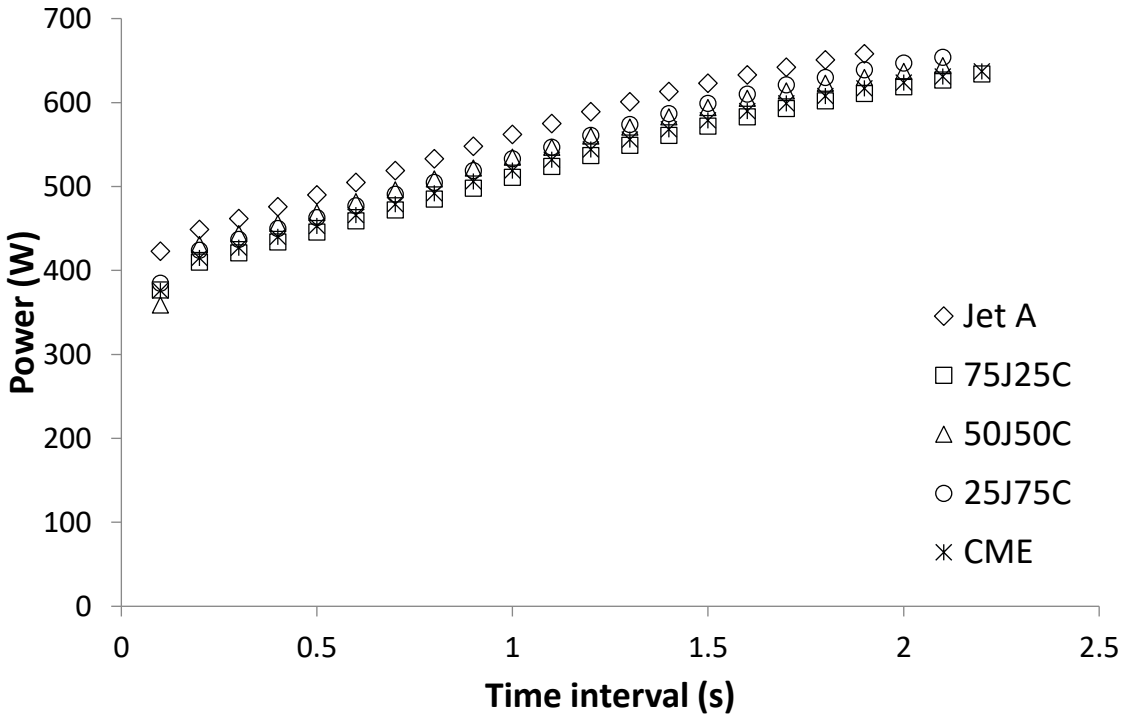

Figure 4.32: Power to the ignitor as a function of time of Jet A – CME Blends at equivalence ratio of 1.30

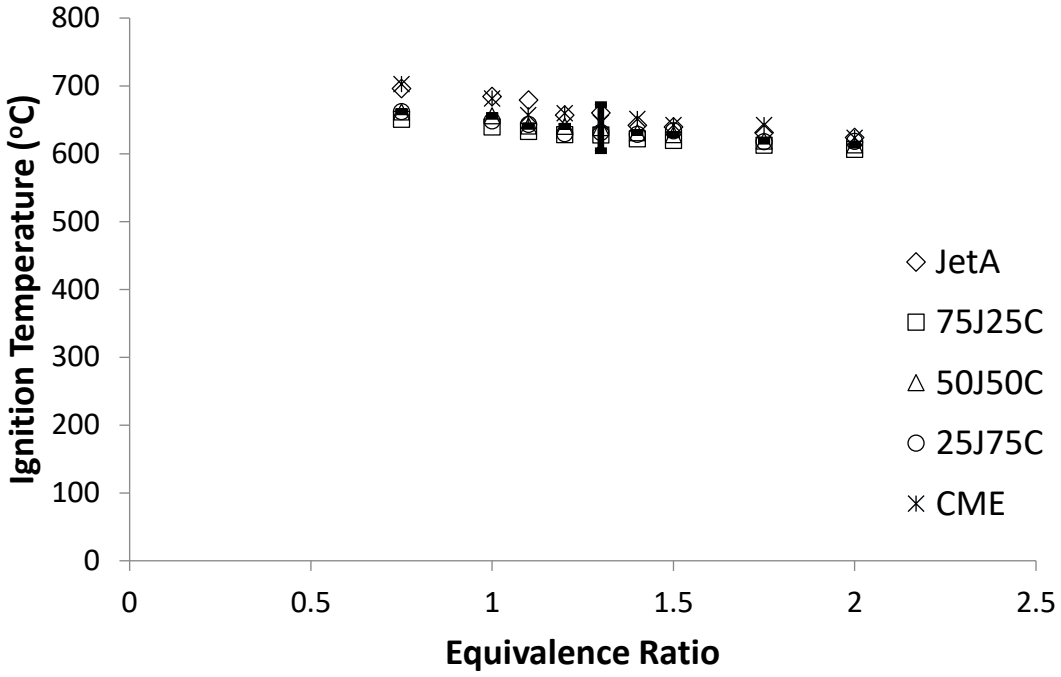

Figure 4.33: Ignition temperature at varying equivalence ratios of Jet A – CME Blends

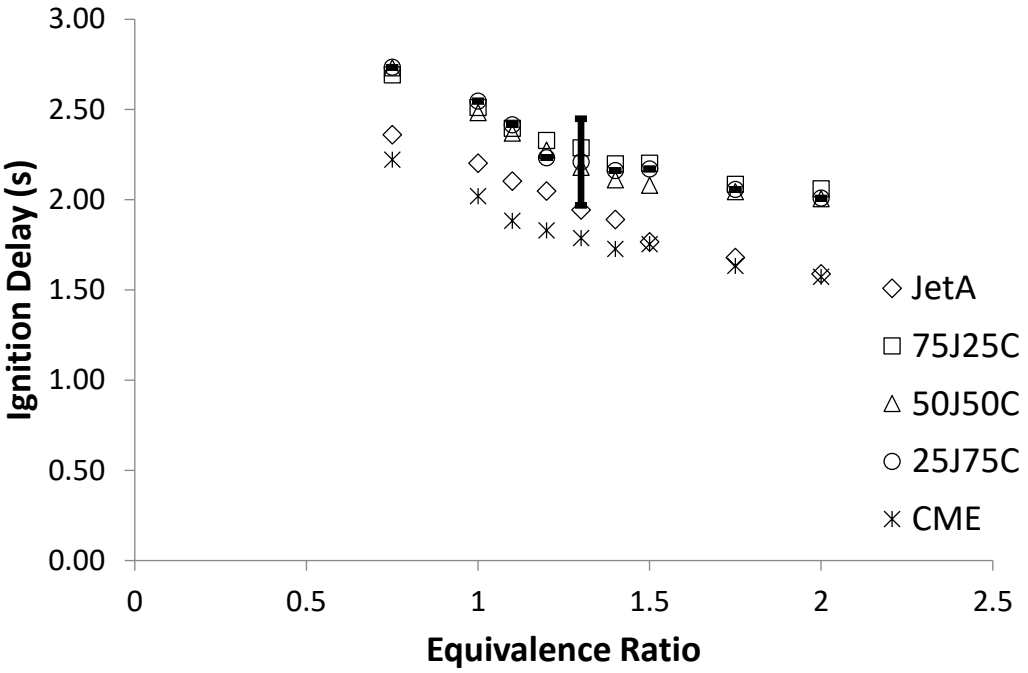

Figure 4.34: Time interval for ignition at varying equivalence ratios of Jet A – CME Blends

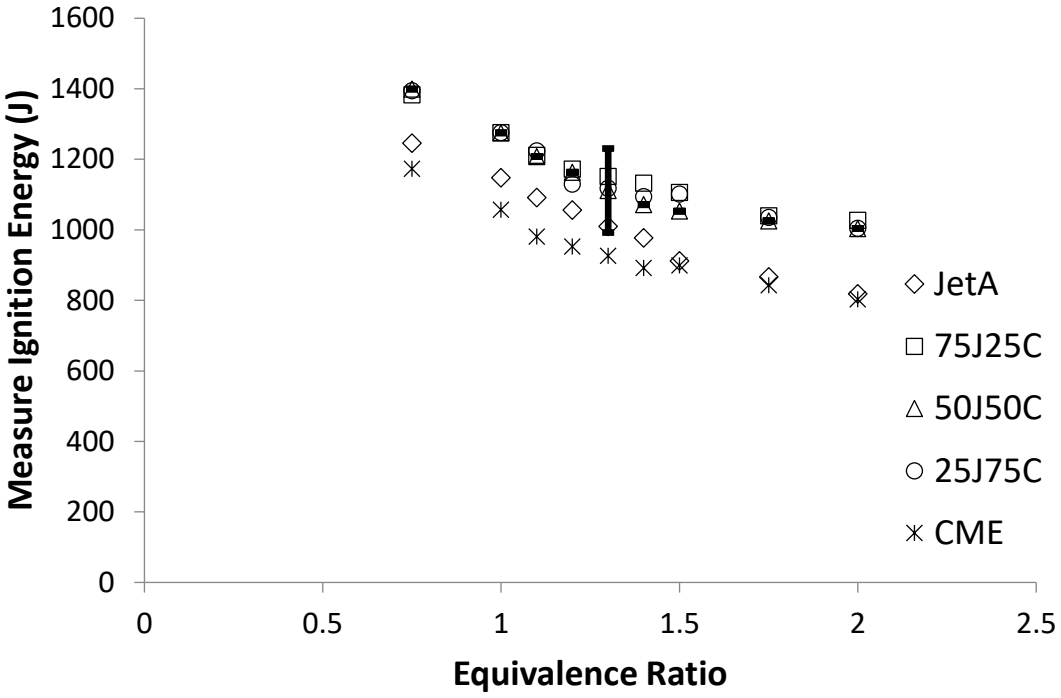

Figure 4.35: Measured ignition energy at varying equivalence ratios of Jet A – CME Blends

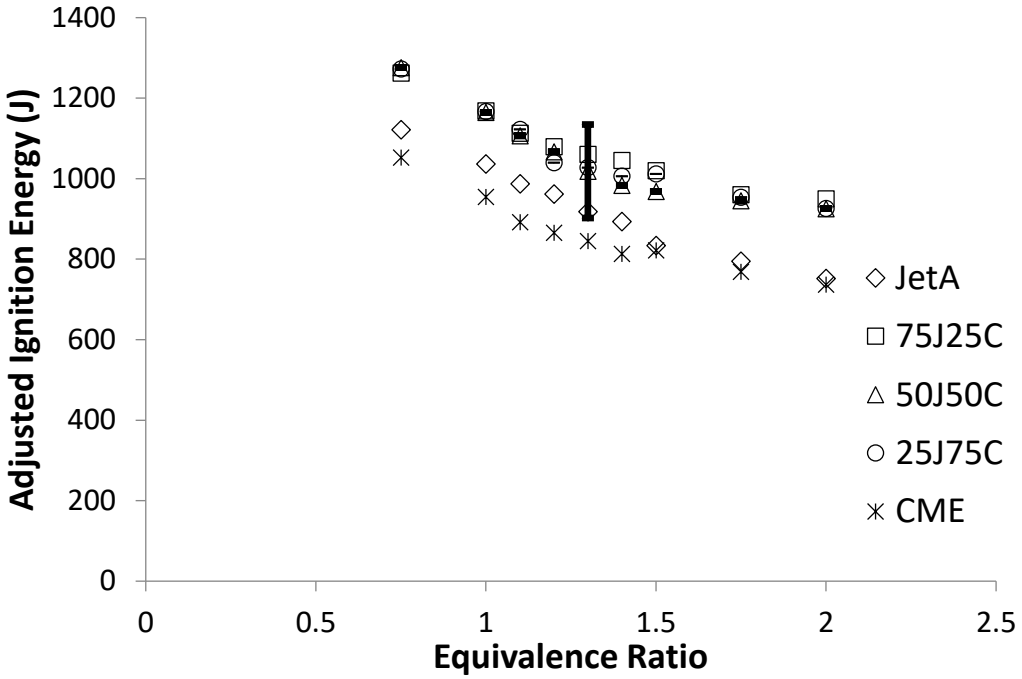

Figure 4.36: Adjusted ignition energy at varying equivalence ratios of Jet A – CME Blends

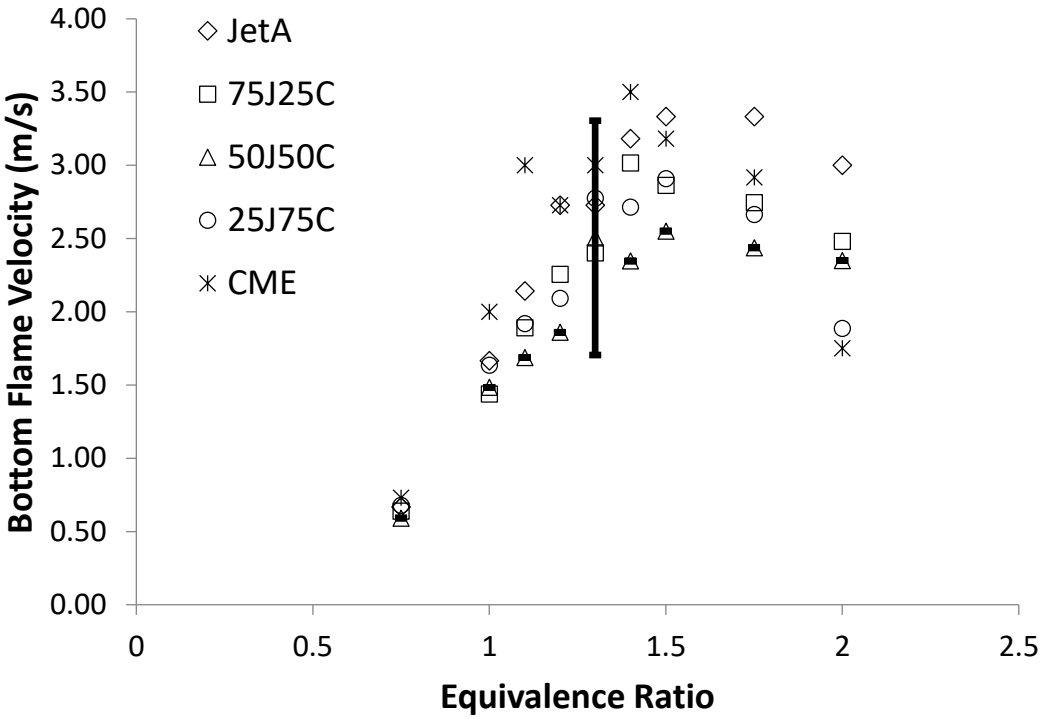

Figure 4.37: Lower flame velocity at varying equivalence ratios of Jet A – CME Blends

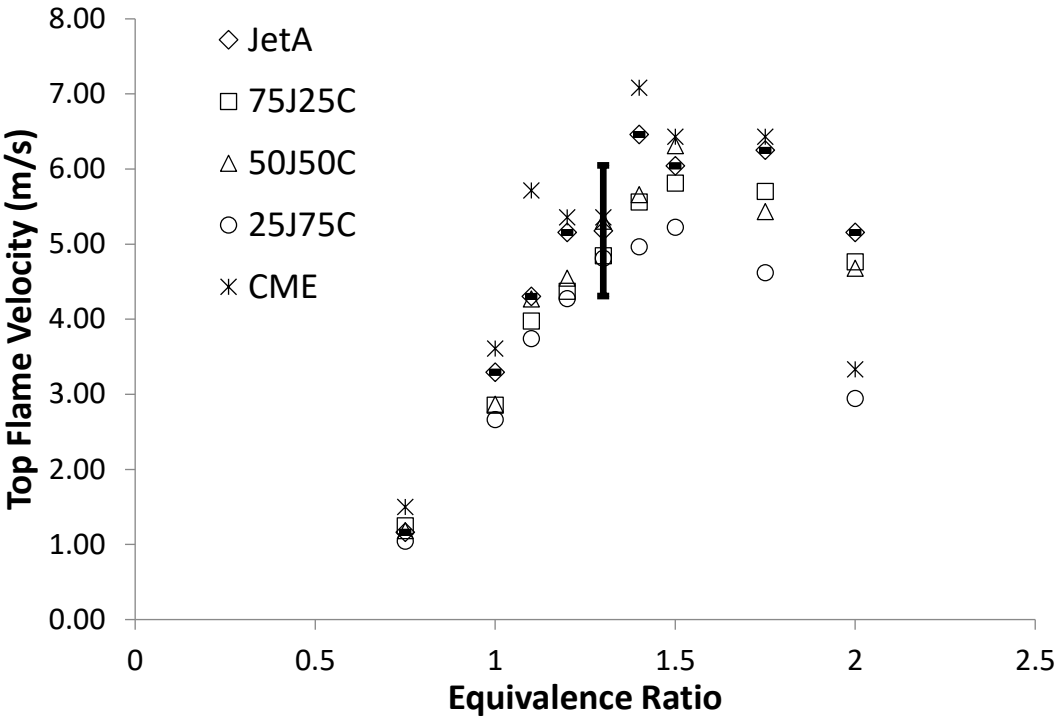

Figure 4.38: Upper flame velocity at varying equivalence ratios of Jet A – CME Blends

CHAPTER 5: SUMMARY AND CONCLUSIONS

In summary, a 1.6 L constant-volume chamber with a hot-surface ignitor was used to measure the fundamental ignition properties of blends of Jet A and CME and Jet A and SME with three different volume ratios over a range of equivalence ratio from 0.75 to 2.00. A hot surface ignition method was used with pre-vaporized liquid fuels in a quasi-stagnant environment. Properties measured included the hot surface ignition temperature, ignition energy, power to ignitor, time interval for ignition, and flame front velocities. Ignition energy and power to ignitor were determined by monitoring the current and voltage supplied to the ignitor. Ignition temperature was calculated using a relationship between the ignitor current and surface temperature. Time interval for ignition was measured as the time between the ignitor start and the first visual appearance of the flame. A high-speed camera at a frame rate of 500 fps was used to measure the flame front velocities as they moved both upwards and downwards. The following conclusions were obtained through measurements and observations:

1. The power supplied to ignitor increased from 350 W to 650 W for the tested fuel. Closer to the ignition point, the power flattened out due to the reduction of heat transfer. Power plots also indicated the time interval for ignition as well as the ignition energy, as calculated by integrating power over time.
2. The hot surface ignition temperatures were constant at about 650°C (923 K) for all fuel blends across various equivalence ratios; this value was comparable to that measured for pure Jet A, SME, and CME. This value was also comparable to that measured with a glowplug for hexane-air mixtures.

3. The values of time interval for ignition and ignition energy were comparable for all fuel blends; the values reached decreased as the equivalence ratio of increased. These values were similar to those obtained for pure Jet A and pure CME; thus, Jet A/CME blends and Jet/SME blends can be handled with the same safety standards at Jet A from an ignition standpoint.
4. The ignition energy was similar between Jet A and biofuels, decreasing with equivalence ratio. After adjustments for energy lost to radiation, the minimum ignition energy occurred at values of approximately 1150 J to 750 J across equivalence ratios.
5. The flame velocities peaked at equivalence ratios of 1.3-1.5 with maximum velocities of around 6.5 m/s upwards and 3.2 m/s downwards; these values were significantly different from the initial flame front velocity due to buoyancy effects. The flame velocities measured were larger than similar studies found in literature due to higher temperatures in the current study and the dependence of flame velocity on temperature.

Recommendations:

The following recommendations are made regarding future research related to the current study:

Examine the ignition properties of other biofuels and tradition fuel blends.

Study the effect of the heating ramp on the ignition energy and time interval for ignition by controlling the ignitor current and temperature.

Model or measure the airflow inside the combustion chamber during the ignition phase to better understand the effects of natural convection on the mixture temperature, ignition energy, and time interval for ignition.

REFERENCES

Agarwal, A. K., 2007. Biofuels (alcohols and biodiesel) applications as fuels for internal combustion engines. *Progress and Energy and Combustion Science*, Volume 33, pp. 233-271.

Balakrishnan, A., Parthasarathy, R. & Gollahalli, S., 2016. Combustion characteristics of partially prevaporized Palm Methyl Ester and Jet-A fuel blends. *Journal of Energy Resources Technology*, Volume 138.

Balakrishnan, A., 2017. *Effects of fuel unsaturation on pollutant emissions from the laminar flames of prevaporized petroleum and biodiesel blends in air*. Norman, Oklahoma.

Bennett, J. & Ballal, D., 2003. Ignition of combustible fluids by heated surfaces. *41st Aerospace Sciences Meeting and Exhibit, Aerospace Sciences Meetings*, () https://doi.org/10.2514/6.2003-148

Boettcher, P. A., 2012. *Thermal Ignition.* Pasadena, California.

Botteri, B. P., Gerstein, M., Horeff, T. & Parker, J., 1979. *Aircraft Fire Safety*.

Cutler, D. P. 1974. Heated surfaces. *Journal of Combustion and Flame*, Volume 22, pp. 105- 109.

Duarte, D. C. D. L., 1994. *Effect of local confinement of the ignition of flammable vapour/air mixture at a hot surface*. Edinburgh, United Kingdom.

Gomez-Meyer, J. S., Gollahalli, S. R., Parthasarathy, R. N. & Quiroga, J. E., 2012. Laminar flame speed of soy and canola biofuels. *Ciencia, Technologia y Futuro*, 4(5), pp. 76-83.

Kermit C. S. & Nelson P. B., 1997. Short-duration autoignition temperature measurements for hydrocarbon fuels near heated metal surfaces. *Combustion Science and Technology*, Volume 126, pp. 225-253.

Kong, D. & Eckhoff, K. R., & Alfert, F. 1995. Auto-ignition of CH4/C3H8/air and CH4/CO2/air using a 11 ignition bomb. *Journal of Hazardous Materials*. Volume 40, pp. 69–84.

Kuchta, J. M. & Cato, R. J., 1966. *Hot Gas Ignition Temperatures of Hydrocarbon Fuel Vapor-Air Mixtures*.

Kuchta, J. M., Bartkowiak, A. & Zabetakis, M. G., 1965. Hot surface ignition temperatures of hydrocarbon fuel vapor-air mixtures. *Journal of Chemical and Engineering Data*, Volume 10, No. 3, pp. 282-288.

Lewis, B. & Von Elbe, G., 1961. *Combustion, flames, and explosions of gases.* New York: Academic Press.

Love, N. D., Parthasarathy, R. N. & Gollahalli, S. R., 2009. Effect of Iodine number on NOx formation in laminar flames of oxygenated biofuels. *International Journal of Green Energy*, 6(4), pp. 323-332.

Johnson, A. M. & Roth, A. J. & Moussa, A., 1988. *Hot Surface Ignition Tests of Aircraft Fluids*.

Ma, J. X. & Alexander, D. & Poulain, D. E., 1998. Laser spark ignition and combustion characteristics of Methane-Air mixtures. *Journal of Combustion and Flame*. Volume 112, pp. 492-502.

Macdonald, J. A. & Cansdale, J. T., 1972. *Spontaneous Ignition of Aircraft Fuel.*

McGary, B. & Steciak, J. & Budwig, R. & Beyerlein, S., 2011. Measuring ignition temperature and the rate of energy generation from Canola Methyl Ester and Soy Methyl Ester in Oxygen-Nitrogen mixtures on Platinum-Rhodium. *International Mechanical Engineering Congress and Exposition.*

Myronuk, D. J., 1980. *Dynamic, Hot Surface Ignition of Aircraft Fuels and Hydraulic Fluids*.

National Biodiesel Board, 2019. *Production Statistics.* [Online] Available at: https://biodiesel.org/production/production-statistics [Accessed 7 May 2019].

Rae, D., Singh, B. & Danson, R., 1964. The size and temperature of a hot square in a cold plane surface necessary for ignition of Methane. *Safety in Mines Research Establishment*, Report Number 224. Sheffield, United Kingdom.

Sheperd, J. E., Krok, J. C. & Lee, J. J., 1999. *Spark Ignition Energy Measurements in Jet A*. California Institute of Technology, Pasadena, California.

Shaw, A. & Epling, W. & McKenna, C. & Weckman, B., 2009. Evaluation of the ignition of diesel fuels on hot surfaces. *Fire Technology*. Volume 46, pp 407-423.

Siccama, N. B. & Westerterp, K. R., 1993. The explosion region becomes smaller under flow conditions: The ignition of Ethane-Air mixture with a hot surface. *Industrial and Engineering Chemistry Research*, Volume 32, Number 7, pp. 1304-1314.

Spens A., Harter J., Parthasarathy R. N. & Gollahalli S. R., 2016. Experimental study of hot surface ignition of prevaporized Jet-A and Canola Methyl Ester. *International Mechanical Engineering Congress and Exposition*.

Spens, A., 2017. Hot surface ignition properties of pre-vaporized Jet-A and biodiesels, Norman, Oklahoma.

Stathopoulos, P., Ninck, K., Rudolf von Rohr, Ph., 2013. Hot-wire ignition of ethanol–oxygen hydrothermal flames. *Journal of Combustion and Flame*, Volume 160, Issue November, pp. 2386-2395.

The Guardian, 2014. *Land taken over by foreign investors could feed 550m people, study finds.* [Online] Available at: https://www.theguardian.com/environment/2014/jun/27/land-grabbing-food-biofuels-crops [Accessed 12 March 2019].

United States Energy Information Administration, 2019. *Monthly Energy Review*. [Online] Available at: https://www.eia.gov/totalenergy/data/monthly [Accessed 4 April 2017].

Zabetakis, M. G., Furno, A. L. & Jones, G.W., 1954. Minimum spontaneous ignition temperatures of combustibles in air. *Industrial and Engineering Chemistry*, Issue October, pp. 2173-2178.

APPENDIX A: NONMENCLATURE

A	Surface area of the ignitor
c	Specific heat of the ignitor
E_{adj}	Adjusted ignition energy
E_C	Energy used to heat up the ignitor
E_i	Ignition energy
E_R	Energy loss due to radiation from ignitor
E_{115V}	Ignition energy corrected for voltage at 115V
E_{120V}	Ignition energy measured at 120V
fps	Frames per second
h	Height
m	Mass of the ignitor
n	Frame number
P_i	Ignitor power output
T_{case}	Temperature inside combustion chamber
T_i	Temperature of the ignitor
t_{ig}	Time of ignition
ΔT	Temperature difference before and after ignition of the ignitor
Δt	Time interval for ignition
V	Flame front velocity
σ	Stefan-Boltzmann constant